Thyroid deficiency before birth alters the adipose transcriptome to promote overgrowth of white adipose tissue and impair thermogenic capacity

Shelley E Harris[1], Miles J De Blasio[2], Xiaohui Zhao[3], Marcella Ma[4], Katie Davies[2], Peter Wooding FBP[2], Russell S Hamilton[3], Dominique Blache[4], David Meredith[1], Andrew J Murray[2], Abigail L Fowden[2] and Alison J Forhead[1,2]

[1]Department of Biological and Medical Sciences, Oxford Brookes University, Oxford, OX3 0BP, UK; [2]Department of Physiology, Development and Neuroscience, University of Cambridge, Cambridge, CB2 3EG, UK; [3]Centre for Trophoblast Research, University of Cambridge, Cambridge, CB2 3EG, UK; [4]Genomics-Transcriptomics Core, Wellcome Trust-MRC Institute of Metabolic Science, University of Cambridge, Cambridge, CB2 0QQ, UK; [5]School of Animal Biology, University of Western Australia, 6009 Crawley, Australia

Short title: Hypothyroidism modifies fetal adipose development

Key words: fetus, thyroid hormone, adipose, insulin, insulin-like growth factor, leptin, uncoupling protein

Abstract

Background Development of adipose tissue before birth is essential for energy storage and thermoregulation in the neonate and for cardiometabolic health in later life. Thyroid hormones are important regulators of growth and maturation in fetal tissues. Offspring hypothyroid *in utero* are poorly adapted to regulate body temperature at birth and are at risk of becoming obese and insulin resistant in childhood. The mechanisms by which thyroid hormones regulate the growth and development of adipose tissue in the fetus, however, are unclear.

Methods This study examined the structure, transcriptome and protein expression of perirenal adipose tissue (PAT) in a fetal sheep model of thyroid hormone deficiency during late gestation. Proportions of unilocular (white) and multilocular (brown) adipocytes, and unilocular adipocyte size, were assessed by histological and stereological techniques. Changes to the adipose transcriptome were investigated by RNA-sequencing and bioinformatic analysis, and proteins of interest were quantified by Western blotting.

Results Hypothyroidism *in utero* resulted in elevated plasma insulin and leptin concentrations and overgrowth of PAT in the fetus, specifically due to hyperplasia and hypertrophy of unilocular adipocytes with no change in multilocular adipocyte mass. RNA-sequencing and genomic analyses showed that thyroid deficiency affected 34% of the genes identified in fetal adipose tissue. Enriched KEGG and gene ontology pathways were associated with adipogenic, metabolic and thermoregulatory processes, insulin resistance, and a range of endocrine and adipocytokine signalling pathways. Adipose protein levels of signalling molecules, including phosphorylated S6-kinase (pS6K), glucose transporter isoform 4 (GLUT4) and peroxisome proliferator-activated receptor γ (PPARγ), were increased by fetal hypothyroidism. Fetal thyroid deficiency decreased uncoupling protein 1 (UCP1) protein and mRNA content, and UCP1 thermogenic capacity without any change in multilocular adipocyte mass.

Conclusions Growth and development of adipose tissue before birth is sensitive to thyroid hormone status *in utero*. Changes to the adipose transcriptome and phenotype observed in the hypothyroid fetus may have consequences for neonatal survival and the risk of obesity and metabolic dysfunction in later life.

Introduction

Congenital hypothyroidism (CH) affects approximately 1 in 2000 neonates worldwide (1). At birth, affected infants are more likely to become hypothermic (1) and a small number of studies have reported that they are at greater risk of obesity, insulin resistance and non-alcoholic fatty liver (NAFL) in childhood and young adult life, even when treated soon after diagnosis (2-6). Low thyroid hormone status in the newborn is also commonly associated with prematurity and intrauterine growth restriction, conditions that have similar consequences for temperature control at birth and long-term metabolic health (7, 8).

Development of adipose tissue before birth is crucial for energy storage, insulation and thermogenesis in the neonatal period and for metabolic health in later life. In the fetus, adipose tissue comprises a mixture of both white and brown adipocyte types (9). White adipocytes, termed unilocular (UL), contain a large single lipid droplet and secrete a variety of adipokines, such as leptin, while brown adipocytes, termed multilocular (ML), are characterised by the presence of several smaller lipid droplets and an abundance of mitochondria with the capacity for non-shivering thermogenesis. Thermogenesis in ML adipocytes is enabled by the unique expression of uncoupling protein 1 (UCP1) on the inner mitochondrial membrane which uncouples the electron transport chain to generate heat.

The sheep fetus is commonly used to study adipose tissue development and thyroid hormone biology before birth. In human and ovine fetuses, adipose tissue first appears around mid-gestation with similar anatomical locations in these and other large mammalian species (10). One of the largest adipose depots is located around the kidneys (perirenal adipose tissue, PAT) which is composed of a mixture of UL and ML adipocytes (10). Towards term, changes in the structure and function of fetal adipose tissue are observed in preparation for the nutritional and thermoregulatory challenges at birth (9). Differential gene expression profiles have been reported in ovine PAT perinatally as the structure of adipose tissue undergoes the transition from

predominantly ML adipocytes at birth to UL adipocyte types at two weeks of postnatal life (9, 11). In fetal sheep, leptin and UCP1 mRNA abundances in PAT increase near term, in association with rising concentrations of cortisol and triiodothyronine (T3) in the circulation (12, 13).

Thyroid hormones, thyroxine (T4) and T3, have important roles in the control of growth, metabolism and development of the fetus (7). In animal models, experimental hypothyroidism *in utero* modifies fetal growth and impairs the maturation and long-term functioning of organs such as the heart, brain and adipose tissue (7). Thyroid deficiency in fetal sheep impairs adipose thermogenic capacity and the ability to maintain body temperature at birth (14). In addition, maternal hypothyroidism during pregnancy increases visceral fat mass and causes glucose intolerance in adult rat offspring (15, 16). Intrauterine programming of adiposity by thyroid hormones has implications for adult insulin sensitivity and metabolic disease (17). Cross-talk between adipose tissue, especially PAT (18), liver and skeletal muscle may be mediated by adipose-derived factors such as free fatty acids and adipocytokines. In adult humans, PAT thickness has been correlated with increased risk of conditions including hypertension, fatty liver and coronary heart disease (18). The molecular mechanisms by which thyroid hormones regulate adipogenesis and adipose function during fetal life, with implications for offspring health in the short and longer term, are, however, poorly understood.

The aims of the current study were to determine the effects of hypothyroidism *in utero* on the growth and development of ovine adipose tissue, and to determine the molecular mechanisms responsible using transcriptome profiling. We tested the hypothesis that thyroid hormone deficiency during late gestation would increase and decrease the amounts of UL and ML adipocytes, respectively, and impair adipose thermogenic capacity near term.

Materials and Methods

Animals

All surgical and experimental procedures were carried out in accordance with UK Home Office legislation and the Animals (Scientific Procedures) Act 1986, after ethical approval by the University of Cambridge Animal Welfare and Ethical Review Body at the Department of Physiology, Development and Neuroscience, University of Cambridge, UK. Nineteen Welsh Mountain pregnant ewes of known gestational age and carrying twin fetuses (15 female and 23 male) were used in this study. The ewes were housed in individual pens and were maintained on 200 g/day concentrates with hay and water *ad libitum* and access to a salt block. Food, but not water, was withheld from the ewes for 18-24 hours before surgery.

Experimental procedures

At 105-110 days of gestation (dGA; term ~ 145 ± 2 days) and under halothane anaesthesia (1.5 % halothane in O_2-N_2O), the twin fetuses of each ewe underwent either a thyroidectomy (TX) or a sham operation in which the thyroid gland was exposed but not removed (sham), as described previously (19, 20). At either 129 (n=18) or 143 dGA (n=20), the fetuses were delivered by Caesarean section under general anaesthesia (20 mg/kg maternal body weight sodium pentobarbitone *i.v.*). Blood samples were collected by venepuncture of the umbilical artery into EDTA-containing tubes. Each fetus was weighed and a variety of fetal organs, including the PAT, were collected after the administration of a lethal dose of barbiturate (200 mg/kg sodium pentobarbitone *i.v.*).

Plasma hormone measurements

Umbilical plasma T3 and T4 concentrations were determined by radioimmunoassay (RIA; MP Biomedicals, Loughborough, UK); the intra-assay coefficients of variation were 3% and 5%, and the minimum levels of detection were 0.14 and 7.0 ng/ml, respectively. Plasma insulin and cortisol concentrations were determined using ELISA kits (insulin: Mercodia, Uppsala, Sweden; cortisol: IBL International, Hamburg, Germany); the intra-assay coefficients of variation were both 9%, and the minimum levels of detection were 0.025 and 2.5 ng/ml, respectively. Plasma

concentrations of leptin, IGF-I and IGF-II were determined by RIA as previously described (21, 22). The intra-assay coefficients of variation were 4-5%, and the minimum levels of detection were 0.09, 0.08 and 4.0 ng/ml, respectively.

Adipose tissue histology

Fetal PAT was fixed in 4 % paraformaldehyde (with 0.2 % glutaraldehyde in 0.1 M phosphate buffer, pH 7.4) and embedded in paraffin wax. Each block of PAT was cut into 7 µm sections and stained with haematoxylin and eosin. Sections were scanned using a NanoZoomer digital slide scanner (Hamamatsu Photonics, Welwyn, UK) to create digital images for analysis. All stereological measurements were performed and analysed blind to the treatment group. The percentage volumes of UL and ML adipocytes were determined using NewCAST stereological software (Visiopharm, Hoersholm, Denmark). A point-counting grid of 25 points was applied over the adipose sections and meander sampling was used to analyse the adipocyte types. A total of 40 counting frames were used per slide to provide at least 200 points per animal. Unilocular cells were defined as an adipocyte with a diameter larger than 60 µm, after tissue shrinkage. Unilocular cell size was determined by measuring the perimeter of 60-80 of the largest UL adipocytes using the stereology software NDP.view2 (Hamamatsu Photonics). Tissue shrinkage was estimated by measurement of the diameter of red blood cells in each section and the perimeter measurements of each fetus were adjusted by 40-50% (23). There was no significant difference in tissue shrinkage between the samples from the TX and sham groups.

RNA-sequencing and bioinformatic analysis

Total RNA was extracted from fetal PAT samples using the RNeasy Lipid Tissue Mini Kit (Qiagen, Manchester, UK) and cDNA libraries were prepared in samples with RIN>6 (Agilent bioanalyser 2100 system, Agilent Technologies TDA UK Limited, Stockport, UK). Briefly, mRNA was enriched from total RNA before reverse transcription, and adenylation and barcode ligation was performed after the synthesis of double stranded cDNA. Ligated libraries were enriched with a

148 limited amplification. Indexed libraries were normalized, pooled and sequenced on the Illumina
149 HiSeq 4000 platform with single end reads (SE50) at the Genomics Core Facility, Cancer Research
150 UK Cambridge Institute, Cambridge, UK.
151 For each library, original reads files were quantified, trimmed and aligned to the Ovis aries
152 (sheep) genome assembly Oar_v3.1 from the International Sheep Genome Consortium using
153 ClusterFlow pipeline tool (version v0.5 dev, fastqc_star pipeline; 24), including the following
154 software: fastqc (version 0.11.5; 25), trim_galore (version 0.4.2; 26), fastq_screen (version 0.9.3;
155 27), MultiQC (version 0.9dev; 28) and read alignment software STAR (version 2.5.1b_modified;
156 29). Further details can be found in the data report (https://github.com/CTR-BFX/2019_AJF).
157 Mapped reads were sorted and indexed with Samtools (30). Subread software (version 1.5.0-p2;
158 31) with the function featureCounts was applied to the indexed bam files to count the mapped
159 reads/fragments per annotated gene from the annotation GTF file provided for the sheep genome
160 (Oar_v3.1) release.
161 As the nucleotide sequences for the thyroid hormone receptor (TR) isoforms, α1 and α2,
162 were not available for sheep, highly similar porcine sequences were used to map their genomic
163 positions in the sheep genome using BLAT (32; https://genome-euro.ucsc.edu/cgi-bin/hgBlat).
164 From the BLAT results, a bed12 file was created to isolate the exon positions for the TRα1 and
165 TRα2 isoforms. Individual RNA-seq alignment files from each of the treatment groups were
166 merged and loaded into Integrative Genomics Viewer (IGV, genome Oar_v3.1).
167 Initial quality control included PCA and data from two fetuses were removed as outliers
168 before further analysis. Differentially expressed genes were identified using R (version 3.5.3)
169 DESeq2 package (version 1.22.2; 33), using variance stabilizing transformed expression for counts.
170 Genes with more than one read across all samples within a contrast were retained. Additional
171 filtering of genes with low mean read counts was automatically applied by DESeq2. For each
172 contrast, differentially expressed genes with Benjamini-Hochberg adjusted P-values < 0.05 were

identified. Log2 fold change in gene expression was plotted against the mean of read counts normalized by library size for each gene in MA plots. Significant differentially expressed genes from each comparison, within and between treatment and gestational age groups, were plotted in volcano plots and a summary of the numbers of genes in the intersections of the comparisons were plotted using UpSetR (version 1.4.0). For heatmap analysis, gene-level transcripts expression values were derived by normalised transformed values estimated by DESeq2 for each sample.

A Bayesian method (lfcshrink) implemented in DESeq2 was used to moderate the log2 fold changes obtained for genes with low or variable expression levels. Upregulated and downregulated genes in different contrasts (BH-adjusted $p < 0.01$ and absolute log2 fold change > 1) were analysed for gene ontology (GO) term enrichment. Gene sets were analysed for over-representation of BP (biological process) and KEGG pathway using R package clusterProfiler (version 3.10.1). Significantly enriched terms were identified by applying the default clusterProfiler algorithm coupled with the Fisher's exact test statistic ($P \leq 0.05$, $q \leq 0.05$). Gene ontology plots were drawn using R package ggplot2 (version 3.2.1). Normalised read counts were used in the statistical analysis of mRNA abundance of key genes. The raw sequencing data and data reports are deposited at ArrayExpress with experimental code E-MTAB-8396. Expression-count data are available online at https://github.com/CTR-BFX/2019_AJF.

Western blotting

Frozen samples of fetal PAT were homogenised in cold lysis buffer (100 mg/ml; 20 mM sodium orthovanadate, 10 mM β-glycerol phosphate, 50 mM sodium fluoride and protease inhibitor cocktail (Roche, Burgess Hill, UK)) in Lysing Matrix-D tubes using a Super FastPrep 1 homogeniser (MP Biomedicals, Loughborough, UK). Samples were centrifuged at 15000g for 10 minutes at 4°C. Extracted protein concentration was measured by a bicinchoninic acid protein assay (Sigma, Poole, UK). Prior to loading, samples were mixed with NuPage 4 x lithium dodecyl sulphate (LDS) loading buffer (2% LDS, 141 mM Tris base, 10% glycerol, 0.51 mM EDTA, 0.22 mM

198 Blue G, 0.175 mM Phenol Red; Life Technologies, Loughborough, UK) and 100 mM DL-
199 dithiothreitol, and heated to 70°C for 10 minutes (with the exception of those for pS6K
200 quantification, which were heated to 99°C for 5 minutes). Equal amounts (100 µg) of sample
201 protein were separated using 7.5% Mini-PROTEAN pre-cast gels (Bio-Rad, Hemel Hempstead, UK)
202 for 50 minutes at 150V and transferred for 10 minutes at 11V onto a polyvinylidene difluoride
203 membrane (Immobilon P 0.45 µm, Millipore, Sigma) using the Pierce G2 Fast Blotter (Thermo
204 Scientific, Loughborough, UK). The membrane was incubated with 2.5% non-fat milk (or bovine
205 serum albumin for phosphorylated proteins) in Tris-buffered saline with 0.1% Tween-20 for 1 hour
206 at room temperature, followed by incubation overnight at 4°C with primary antibodies: rabbit
207 polyclonal anti-InsRβ (10 µg/ml, Santa Cruz Biotechnologies, Heidelberg, Germany), rabbit
208 polyclonal anti-IGF-1Rβ (10 µg/ml, Santa Cruz Biotechnologies), rabbit polyclonal anti-leptin
209 receptor (1 µg/ml, Biorbyt, Cambridge, UK), rabbit polyclonal anti-pAkt (1:800, Ser473, Cell
210 Signalling Technology, Hitchin, UK), mouse monoclonal anti-Akt1 (1:1000, Cell Signalling
211 Technology), rabbit monoclonal anti-Akt2 (1:1000, Cell Signalling Technology), rabbit polyclonal
212 anti-pmTOR (1:800, Ser 2448, Cell Signalling Technology), rabbit polyclonal anti-pS6K (1:1000, Thr
213 389, Cell Signalling Technology), rabbit polyclonal anti-GLUT4 (2.5 µg/ml, Abcam, Cambridge, UK),
214 mouse monoclonal anti-PCNA (2 mg/L, Dako, Cambridge UK), rabbit polyclonal anti-PPARγ (4
215 µg/ml, Biorbyt) and rabbit polyclonal anti-UCP1 (1:500, Abcam). Each membrane was incubated
216 with a horseradish peroxidase-conjugated anti-rabbit or anti-mouse secondary antibody (GE
217 Healthcare, Amersham, UK) for 1 hour at room temperature. Protein expression was visualised by
218 addition of Clarity Western ECL chemiluminescence substrate (Bio-Rad, Hemel Hempstead, UK)
219 and quantified using Image Lab software (ChemiDoc, Bio-Rad) after normalisation to Ponceau S
220 staining (34). All data were normalised to a quality control sample across all gels and expressed as
221 fold changes, relative to the sham group at 129 dGA, in arbitrary units.
222

Citrate synthase activity

Citrate synthase (CS) activity was measured in homogenised PAT samples by a spectrophotometric enzyme assay. The assay buffer (pH 8) contained 0.1 mM 5,5'-dithio-bis-2-nitrobenzoic acid, 1 mM oxaloacetate and 0.3 mM acetyl-CoA. Adipose CS activity was determined from the maximum rate of change of absorbance at 412 nm and 37°C (rate of thionitrobenzoic acid production) over 3-minute periods and was expressed as µmoles per minute per mg protein, measured by a bicinchoninic acid protein assay.

Statistical methods

Data were analysed by three-way ANOVA with treatment, gestational age and sex of the fetus as factors (SigmaStat 3.5, Systat Software, San Jose, California, USA). The sex of the fetus had no significant effect on any of the variables measured; data from male and female fetuses were, therefore, combined and analysed by two-way ANOVA followed by the Tukey *post-hoc* test. Relationships between variables were assessed by Pearson's correlation. Significance was regarded as $P<0.05$.

Results

Hypothyroidism *in utero* increases circulating insulin and leptin concentrations

In TX fetuses, plasma T4 and T3 concentrations decreased to below the limits of assay detection, while plasma insulin and leptin were increased to levels above those in sham fetuses at both 129 and 143 days of gestation (dGA; $P<0.05$; Table 1). The normal developmental rise in plasma cortisol concentration over this time period was observed in both groups of fetuses ($P<0.05$; Table 1); fetal hypothyroidism tended to suppress plasma cortisol concentration ($P=0.052$). Plasma T3 increased near term in the sham fetuses ($P<0.05$; Table 1), while plasma concentrations of IGFI and IGFII were unaffected by TX or gestational age (Table 1).

UL-specific adipocyte growth and proliferation enlarges adipose tissue mass in hypothyroid fetuses

In TX fetuses, absolute PAT weight was greater than in sham fetuses at 143 dGA ($P<0.05$), but not 129 dGA (Table 1); the PAT mass relative to body weight was higher in TX than sham fetuses at both ages ($P<0.05$, Table 1). When expressed as a percentage of total PAT volume, sham fetuses had a greater percentage of ML relative to UL adipocyte types at 129 and 143dGA ($P<0.001$, Figure 1A). In TX fetuses, there was an increase in the percentage of UL, and a decrease in ML, adipocytes compared to control values at both ages ($P<0.001$; Figure 1A). When the percentage volumes of ML and UL adipocytes were expressed as absolute and relative masses, a 0.95-1.30-fold increase in UL adipocyte mass was observed in the TX fetuses at both 129 and 143dGA ($P<0.05$, Figure 1B). The absolute and relative ML adipocyte masses, and fetal body weight, were unaffected by TX (Table 1, Figure 1B). Positive correlations were observed between the relative UL adipocyte mass and fetal concentrations of insulin ($R=0.49$, $N=37$, $P<0.005$) and leptin ($R=0.68$, $N=38$, $P<0.001$). The average perimeter of the largest UL adipocytes increased with hypothyroidism ($P<0.05$) and gestational age ($P<0.001$; Figure 1C). These data indicate that the increase in PAT mass observed after TX was due to increased UL-specific adipocyte growth and proliferation (Figure 1D and E).

Adipose transcriptome analysis reveals differential gene expression profiles in response to hypothyroidism *in utero*

RNA-sequencing was undertaken on PAT samples from sham and TX fetuses at both 129 and 143 dGA and the distribution of gene expression was assessed initially by unbiased principal component analysis (PCA). Using the top 500 most variable genes, PCA showed distinct clustering of data based on treatment group (sham and TX) and common transcriptional profiles between gestational age within treatment groups (Supplementary Figure 1A). Genes associated with the effect of TX, defining the principal component 1 (PC1), explained 43.5% of the variance. These

included *LPL, ELOVL6, PLIN1, FBP2* and *ADIPOQ* (Supplementary Figure 1B). Genes associated with the effect of gestational age within each treatment group (principal component 2, PC2) explained 14.0% of the variance and included *UCP1, DIO1, FABP3* and *ADRA1A* (Supplementary Figure 1C). A hierarchical clustering heatmap using 272 differentially expressed genes with an absolute log2 fold change threshold of 2 and P-adjusted < 0.05 confirmed that the transcriptome data from the sham and TX groups clustered apart (Supplementary Figure 1D).

In total, 17622 genes were identified in the adipose samples from the annotated sheep genome. Of these, 5999 genes were differentially expressed between the sham and TX groups (34.0%, P-adjusted < 0.05). When data from all animals were considered with an absolute log2 fold change ≥ 1, a total of 1472 genes were affected by hypothyroidism (768 up and 704 down-regulated by TX; Supplementary Figure 2A) and 409 were affected by increasing gestational age (180 up, 229 down with increased gestational age; Supplementary Figure 2B). When the data were analysed by age in each treatment group, the expression of 609 genes changed between 129 and 143 dGA in the sham fetuses (232 up, 377 down; Supplementary Figure 2C), while this number was reduced to 174 in the TX fetuses over the same time period (86 up, 88 down; Supplementary Figure 2D). When the data were analysed by treatment at each age, TX influenced the expression of more genes at 143 dGA (1576 total, 869 upregulated, 707 downregulated; Supplementary Figure 2F) than at 129 dGA (1090 total, 625 upregulated, 465 downregulated; Supplementary Figure 2E). Transcriptome profiles were compared between and within treatment and gestational age groups and the results are summarised in the UpSet plot (Supplementary Figure 3A). Differentially expressed genes unique to each of the comparisons were also plotted (Supplementary Figure 3B).

Gene ontology and KEGG pathway analyses identify adipogenic, metabolic, thermogenic and hormone signalling processes influenced by hypothyroidism *in utero*

296 A number of biological pathways were identified as enriched in PAT from TX fetuses. Of
297 particular relevance, enriched KEGG pathways were associated with regulation of lipolysis; fatty
298 acid synthesis and metabolism; insulin resistance; AMPK, FoxO and cAMP signalling; and signalling
299 pathways for insulin, peroxisome proliferator-activated receptor (PPAR) and adipocytokines
300 (Figure 2A and Supplementary Figure 4). Biological process pathways over-represented in the
301 gene ontology analysis included fatty acid metabolism and biosynthesis, and several aspects of
302 thermogenesis and temperature regulation (Figure 2B and Supplementary Figure 5). When the
303 data were assessed by treatment and age, an additional number of enriched pathways were
304 identified in TX fetuses at 129 dGA including apelin and thyroid hormone signalling pathways
305 (Supplementary Figure 4) and lipid metabolism (Supplementary Figure 5).

306 **Hypothyroidism *in utero* activates adipose PPAR and insulin-IGF signalling**

307 Key genes in some of the enriched pathways were examined in more detail and protein
308 content was quantified by Western blotting. Increased mRNA and protein contents of the mitotic
309 marker, proliferating cell nuclear antigen (PCNA), and PPARγ, an important regulator of adipocyte
310 differentiation, were observed in response to fetal hypothyroidism ($P<0.005$, Supplementary
311 Figure 6A and B). Adipose PCNA mRNA abundance decreased between 129 and 143 dGA in sham
312 fetuses ($P<0.05$), and PCNA mRNA and protein contents were higher in TX compared sham fetuses
313 at 143 dGA ($P<0.05$; Supplementary Figure 6A). Compared with control values, both the mRNA
314 and protein contents of PPARγ at 129 dGA, and mRNA abundance at 143 dGA, were greater in TX
315 fetuses ($P<0.05$; Supplementary Figure 6B). Adipose mRNA abundances of IGFI and IGFII and
316 leptin were also increased by TX ($P<0.001$, Supplementary Figure 7A, B and C). An increase in
317 adipose IGFI mRNA was observed between 129 and 143 dGA in TX fetuses ($P<0.05$; Supplementary
318 Figure 7A); over the same period, IGFII mRNA abundance decreased in both sham and TX fetuses
319 ($P<0.05$; Supplementary Figure 7B).

To examine if hyperinsulinemia and increased adipose IGF mRNA abundance observed in TX fetuses were responsible, at least in part, for the greater PAT mass, the expression of insulin-IGF and adipokine signalling pathways were investigated in sham and TX fetuses. At 129 dGA, the mRNA abundance of the insulin receptor was higher, while insulin receptor β-subunit (InsRβ) protein content was lower in TX fetuses compared to sham fetuses ($P<0.05$, Supplementary Figure 6C). Between 129 and 143 dGA, a reduction in InsRβ protein was seen in sham, but not TX fetuses ($P<0.05$, Supplementary Figure 6Cii). At 129 dGA, protein kinase β 1 (Akt1) and Akt2 mRNA, and Akt1 protein content, were greater in TX compared to sham fetuses ($P<0.05$, Supplementary Figure 6D-E). In the TX fetuses, Akt2 mRNA abundance decreased between 129 and 143 dGA, and Akt2 protein content was lower at 143 dGA compared to that observed in sham fetuses ($P<0.05$, Supplementary Figure 6E). The total amount of phosphorylated Akt (pAkt) protein did not change with age or fetal hypothyroidism (data not shown).

A developmental rise in mRNA abundance of the mammalian target of rapamycin (mTOR) was observed in sham, but not TX fetuses ($P<0.05$, Supplementary Figure 6Fi); at 143 dGA only, mTOR mRNA abundance was lower in TX than sham fetuses ($P<0.05$, Supplementary Figure 6Fi). Fetal hypothyroidism reduced phosphorylated mTOR protein content ($P<0.05$), although *post-hoc* analysis failed to identify significant differences at either age (Supplementary Figure 6Fii). At 129 dGA, phosphorylated S6 kinase (pS6K) protein content was higher in TX than sham fetuses ($P<0.05$), and decreased with increasing age in TX but not sham fetuses ($P<0.05$, Supplementary Figure 6Gii); S6K mRNA abundance, however, was unaffected by fetal TX and age (Supplementary Figure 6Gi). In TX fetuses, mRNA abundance of the insulin-sensitive glucose transporter, GLUT4, was greater than that observed in sham fetuses at 129 dGA and decreased towards term, unlike sham fetuses ($P<0.05$, Supplementary Figure 6Hi). Adipose GLUT4 protein content was also greater in TX than sham fetuses at both ages ($P<0.05$, Supplementary Figure 6Hii).

Developmental increments in adipose adrenergic receptor (ADR) α1A mRNA abundance were observed between 129 and 143 dGA in both sham and TX fetuses, without any effect of TX ($P<0.05$, Figure 5D). Adipose ADRβ2 mRNA abundance also increased towards term in sham but not TX fetuses; ADRβ2 mRNA abundance was lower in TX compared to sham fetuses at 143 dGA ($P<0.05$, Supplementary Figure 7H). At 129 dGA, the mRNA abundance of ADRα1D was lower, while that of ADRβ1 and ADRβ3 were all higher, in TX than sham fetuses ($P<0.05$, Supplementary Figure 7E, G and I). Adipose ADRα2A was increased by TX at both 129 and 143 dGA ($P<0.05$, Supplementary Figure 7F). There were no effects of TX or age on the amount of the long-form leptin receptor protein, ADRα1B mRNA abundance, or the mRNA or protein abundance of the IGF type 1 receptor in PAT (data not shown).

Hypothyroidism *in utero* impairs adipose thermogenic capacity

Although the absolute and relative masses of ML adipocytes were unaffected by TX, the capacity for non-shivering thermogenesis was impaired in the PAT of TX fetuses. Adipose citrate synthase (CS) activity, as a proxy measure of mitochondrial density, increased between 129 and 143 dGA in sham but not TX fetuses ($P<0.05$, Table 1); CS activity in the TX fetuses was lower than control values at both ages ($P<0.05$, Table 1). When observations from all fetuses were considered, regardless of gestational age or treatment group, a positive relationship was observed between adipose CS activity and the percentage volume of ML adipose tissue ($R=0.53$, $N=37$, $P<0.001$). Both adipose UCP1 mRNA and protein content (both absolute values and when expressed relative to CS activity or percentage volume of ML adipose tissue) increased near term in sham fetuses, but these developmental changes were abolished by TX (Figure 3). Absolute and relative UCP1 mRNA abundance was lower in TX compared to sham fetuses at 143 dGA ($P<0.05$, Figure 3A and B); relative UCP1 protein content was reduced by TX at both 129 and 143 dGA ($P<0.05$, Figure 3C and D) in line with previous findings at term (7).

Hypothyroidism *in utero* alters adipose thyroid hormone metabolism and signalling

Adaptive changes in adipose mRNA abundance for the iodothyronine deiodinases (DIO) and thyroid hormone receptors (TR) were observed in response to TX. Towards term, significant increments in the mRNA abundance of DIO1 and DIO2, which both metabolise T4 to the biologically active T3, were observed in sham but not TX fetuses ($P<0.05$, Figure 4A and B). In TX fetuses, lower DIO1 mRNA level at 143 dGA, and higher DIO2 mRNA level at 129 dGA, were observed compared to the sham fetuses ($P<0.05$, Figure 4A and B). Adipose mRNA levels of TRα1, TRα2 and TRβ were increased by TX at both ages ($P<0.05$, Figure 4C, D and E); a significant increase in adipose TRβ mRNA was observed in sham fetuses near term ($P<0.05$, Figure 4E). A Sashimi plot was constructed to show the expression of the splice variants TRα1 and TRα2 (Supplementary Figure 8) and adipose TRα1 and α2 mRNA levels were highly correlated when data from all animals were combined ($R=0.99$, $N=35$, $P<0.0001$).

Discussion

This study has shown for the first time that thyroid hormone deficiency modifies the transcriptome, and hence the growth and development of fetal adipose tissue, in a manner that is likely to compromise the ability of the neonate to maintain body temperature at birth and to increase its risk of metabolic dysfunction in later life. Fetal hypothyroidism caused a shift in the relative composition of UL and ML adipocyte types towards an increase in UL adipocyte mass due to hyperplasia and hypertrophy. Gene markers of UL adipocyte type, such as leptin, adiponectin and lipoprotein lipase, were increased in TX ovine fetuses, and adipocyte proliferation was indicated by elevated levels of the mitotic marker PCNA and enrichment of gene pathways responsible for PPARγ and insulin-IGF signalling. The percentage of ML adipocytes in PAT was reduced by hypothyroidism *in utero* and, although the total amount of ML adipose tissue did not differ between sham and TX fetuses, UCP1 expression was impaired, when normalised to mitochondrial density estimated by CS activity, indicating a deficit in thermogenic capacity. Furthermore, bioinformatic analysis showed that, for a substantial number of genes,

394 hypothyroidism prevented the maturational changes normally seen in the transcriptome of ovine
395 PAT near term.
396 The effects of thyroid hormone deficiency on adipose tissue development before birth may
397 be direct, via thyroid hormone response elements on target genes (17), and/or indirect, via
398 changes to energy expenditure and by interactions with other nuclear receptors or changes in
399 fetal hormone concentrations, such as insulin and the IGFs. Basal metabolic rate is difficult to
400 measure *in utero*, but previous studies have shown that thyroid hormone deficiency in the sheep
401 fetus reduces the whole-body rate of oxygen consumption and is normalised by T4 replacement
402 (35). The extent to which changes in global energy expenditure induced by hypothyroidism
403 contribute to the modifications in the growth and development of fetal PAT in the present study
404 remain to be determined.
405 The increased circulating concentration of insulin seen in the hypothyroid sheep fetus,
406 secondary to pancreatic β-cell proliferation (20), is likely to be responsible, at least in part, for UL-
407 specific PAT overgrowth. Indeed, a positive correlation was observed between fetal insulin
408 concentration and relative UL adipocyte mass in the present study. Before birth, insulin stimulates
409 growth of the axial skeleton and tissues such as adipose tissue (36). In the ovine fetus,
410 hyperglycemia and hyperinsulinemia induced by fetal glucose infusion have also been shown to
411 promote UL adipocyte growth with no change in ML adipocyte mass (37). A variety of signalling
412 pathways responsive to insulin and the IGFs, and known to be involved in the control of
413 adipogenesis, were enriched in the adipose transcriptome by hypothyroidism *in utero*. These
414 included PPARγ, apelin and FoxO signalling. Furthermore, measurement of selected downstream
415 target proteins showed upregulation of pS6K, GLUT4 and PPARγ in TX fetuses. Phosphorylation of
416 S6K, without any change in mRNA abundance, indicated activation of the PI3-kinase pathway
417 which is known to regulate adipogenesis via a range of transcription factors and interacting
418 molecular pathways (38, 39). Transgenic mice with mutation in the S6K gene are growth retarded

419 from embryonic life with reductions in pancreatic β-cell size and insulin content (40). This
420 phenotype persists to adulthood and is associated with impaired adipogenesis, increased insulin
421 sensitivity and resistance to diet-induced obesity (41). Increased adipose GLUT4 expression in TX
422 sheep fetuses may also contribute to adipogenesis via enhanced glucose uptake and lipid storage
423 and are consistent with findings in rat pups hypothyroid in fetal and neonatal life (42).
424
425 While circulating IGF levels remained unchanged in TX sheep fetuses, adipose mRNA
426 abundances for IGFI and II were elevated, indicating potential upregulation of local synthesis and
427 paracrine actions of the IGFs. Thyroid hormone deficiency *in utero* has been shown previously to
428 modify IGF expression in liver and skeletal muscle with tissue-specific effects on growth and
429 development in fetal sheep (43, 44). Insulin-IGF signalling pathways can also induce the synthesis
430 of adipokines, such as leptin, apelin and adiponectin, in part via interactions with PPARγ signalling.
431 Previous studies have shown that hyperinsulinaemia, in the presence of euglycaemia, increases
432 adipose leptin mRNA abundance in fetal sheep (45). High circulating levels of thyroid-stimulating
433 hormone associated with TX may also stimulate leptin secretion, as reported in human adipose
434 tissue cultured *in vitro* (46). The extent to which the increase in adipose adipokine expression and
435 circulating leptin levels in the hypothyroid sheep fetus result from the greater UL adipocyte mass
436 and/or greater capacity for adipokine synthesis and secretion in individual UL adipocytes remains
437 to be established.
438 Thyroid deficiency *in utero* reduced adipose UCP1 expression and affected several genes in
439 the thermogenic pathway, without changing ML adipocyte mass. Previous studies have shown
440 that hypothyroid lambs are unable to maintain normal body temperature at delivery and their PAT
441 contains less UCP1 and more lipid (14). Maternal hypothyroidism in rats led to low adipose UCP1
442 mRNA abundance in the fetuses which correlated with adipose T3 levels and was corrected by
443 maternal thyroid hormone treatment (47). Furthermore, in cultured brown adipocytes taken from

444 fetal rats, T3 causes an increase in UCP1 gene transcription, mRNA stability and mitochondrial
445 protein content (48). Moreover, a thyroid hormone response element (TRE) has been reported
446 upstream of the promoter region of the UCP1 gene (49). Suppression of adipose UCP1 levels were
447 observed in TX sheep fetuses despite upregulation of other factors known to stimulate UCP1
448 expression, such as ADRβ3, IGFI, leptin and PPARγ, possibly as compensatory mechanisms. The
449 sympathomedullary system is primarily activated at birth by delivery into a cold environment and
450 normally interacts with thyroid hormones to promote UCP1 expression and non-shivering
451 thermogenesis. Although plasma catecholamine concentrations were not measured in the
452 present study, PAT catecholamine content has been reported to be unaffected by TX in fetal sheep
453 (50). Previous studies have also shown that noradrenergic-induced cellular respiration in PAT is
454 suppressed in TX sheep fetuses, compared with those infused with T3, which suggests that
455 functional adrenergic signalling may be impaired, despite elevated PAT mRNA abundance of some
456 ADR isoforms (51). The effects of hypothyroidism *in utero* may also originate from abnormal
457 formation of hypothalamic pathways responsible for adipose thermogenesis, especially since
458 thyroid hormones have a key role in the development of the fetal brain (52).
459 Maturational changes in thyroid hormone metabolism and signalling were observed in fetal
460 adipose tissue during late gestation, which were modified by thyroid hormone deficiency. In sham
461 fetuses, mRNA abundances of iodothyronine deiodinases DIO1 and DIO2, and the thyroid
462 hormone receptor TRβ, increased towards term. Upregulation of DIO1 and DIO2 enzyme activities
463 have been demonstrated previously in ovine fetal PAT over the same period of gestation, in part
464 due to the prepartum rise in plasma cortisol (53, 54). Increased DIO1 enzyme activity in the PAT,
465 and liver and kidney, of the sheep fetus near term are likely to be responsible for the increase in
466 plasma T3 seen close to term (54). Hypothyroidism *in utero* had contrasting effects on the
467 expression of DIO1 and DIO2 mRNA in ovine fetal PAT: DIO1 was reduced to negligible levels and
468 DIO2 was increased in TX fetuses, in line with previous findings on deiodinase enzyme activity in

adipose and other tissues of hypothyroid sheep and rat fetuses (47, 53, 55). Indeed, bioinformatic analysis identified DIO1 as the top-ranked gene affected by fetal TX in the current study with a 7.4-fold decrease in expression levels. Although DIO2 enzyme activity is much lower than DIO1 in ovine fetal PAT (54), the increase in DIO2 mRNA abundance may be an adaptive response to maintain local T3 production in hypothyroid conditions. The molecular mechanisms responsible for the tissue-specific control of deiodinase expression by thyroid hormone deficiency before birth remain to be established, although a TRE has been identified in the human Dio1 gene (56). Within the PAT of TX sheep fetuses, the mRNA abundances of both thyroid hormone receptors, TRα and β, were increased in an apparent attempt to maintain local sensitivity to thyroid hormones in the face of systemic hypothyroidism. Fetal thyroid hormone deficiency appeared to upregulate TRα gene expression without affecting the relative proportions of the splice variants α1 and α2.

During hypothyroidism *in utero*, activation of adipogenesis, suppression of thermogenic capacity, and exposure of the fetus to high circulating levels of insulin and adipocytokines may have consequences for adipose function and insulin sensitivity in the longer term (8). Human infants exposed to hyperinsulinemia before birth, such as those born to obese mothers, have greater percentage body fat, higher umbilical cord leptin concentration and raised indicators of insulin resistance compared to those born to lean mothers (57). In the present study, genomic pathways associated with insulin resistance were identified as enriched in PAT from TX fetuses. Furthermore, since there is a link between adiposity in the neonate and child (58), these findings suggest that the development of fetal adipose tissue and enhancement of insulin resistance pathways may predispose offspring hypothyroid *in utero* to obesity and metabolic disease in later life. Several studies worldwide have shown that children born with CH have a greater body mass index and are more at risk of obesity, insulin resistance and NAFL in early and young adult life compared with the general population, even when diagnosed and treated with T4 soon after birth (2-6). Moreover, infants with more moderate reductions in thyroid hormones associated with

494 prematurity or intrauterine growth retardation are also at greater risk of obesity and
495 cardiometabolic dysfunction in later life (7, 8). Collectively, these findings suggest that exposure
496 to hypothyroidism *in utero* permanently alters adipose tissue development with consequences for
497 adult health. Further investigations are required, however, to determine whether these
498 programming effects arise directly from the altered adipose phenotype and/or indirectly from
499 other changes in endocrine activity, metabolism or appetite regulation that affect adult adiposity.
500 For example, antithyroid drug treatment in pregnant rats leads to hyperleptinaemia in the adult
501 offspring and alterations in hypothalamic leptin signalling molecules indicative of leptin resistance
502 (59). Hyperinsulinaemia and overgrowth of UL adipose tissue in sheep fetuses infused with
503 glucose were also associated with changes to the expression of neuropeptides in the appetite-
504 regulatory regions of the hypothalamus (37). Elucidation of the molecular pathways influenced by
505 thyroid deficiency *in utero*, and the long-term consequences for physiological function in a range
506 of tissues, will enable greater understanding of the health outcomes in offspring exposed to
507 hypothyroidism before birth.
508
509

Acknowledgments

The authors would like to thank technical staff at the Universities of Cambridge, Oxford Brookes and Western Australia for their assistance in the study. The project was funded in part by the Biotechnology and Biological Sciences Research Council, and a Research Excellence Award from Oxford Brookes University to AJF. SEH was supported by a Nigel Groome PhD Studentship, Oxford Brookes University. Sample library preparation and RNA-seq work were performed at the Genomics and Transcriptomics core, which is funded by the UK Medical Research Council (MRC) Metabolic Disease Unit (MRC_MC_UU_12012/5) and a Wellcome Trust Major Award (208363/Z/17/Z).

Corresponding author: Dr Alison J Forhead, Department of Physiology, Development and Neuroscience, University of Cambridge, Cambridge, CB2 3EG, UK; +44 1223 333853; ajf1005@cam.ac.uk

525 **References**

526 1. Wassner AJ 2018 Congenital hypothyroidism. Clin Perinatol 45:1-18.

527 2. Wong SC, Ng SM, Didi M 2004 Children with congenital hypothyroidism are at risk of adult

528 obesity due to early adiposity rebound. Clin Endocrinol 61:441-446.

529 3. Arenz S, Nennstiel-Ratzel U, Wildner M, Dörr HG, von Kries R 2008 Intellectual outcome, motor

530 skills and BMI of children with congenital hypothyroidism: a population-based study. Acta Paediatr

531 97:447-450.

532 4. Léger J, Ecosse E, Roussey M, Lanoë JL, Larroque B 2011 Subtle health impairment and

533 socioeducational attainment in young adult patients with congenital hypothyroidism diagnosed by

534 neonatal screening: a longitudinal population-based cohort study. J Clin Endocrinol Metab

535 96:1771-1782.

536 5. Chen SY, Lin SJ, Lin SH, Chou YY 2013 Early adiposity rebound and obesity in children with

537 congenital hypothyroidism. Pediatr Neonatol 54:107-112.

538 6. Pan YW, Tsai MC, Yang YJ, Chen MY, Chen SY, Chou YY 2019 The relationship between

539 nonalcoholic fatty liver disease and pediatric congenital hypothyroidism patients. Kaohsiung J.

540 Med. Sci. doi: 10.1002/kjm2.12118.

541 7. Forhead AJ, Fowden AL 2014 Thyroid hormones in fetal growth and prepartum maturation. J

542 Endocrinol 221:87-103.

543 8. Meas T 2010 Fetal origins of insulin resistance and the metabolic syndrome: a key role for

544 adipose tissue? Diabetes Metab 36:11-20.

545 9. Pope M, Budge H, Symonds ME 2014 The developmental transition of ovine adipose tissue

546 through early life. Acta Physiol 210:20-30.

547 10. Symonds ME, Pope M, Budge H 2015 The ontogeny of brown adipose tissue. Annu Rev Nutr

548 35:295-320.

549 11. Basse AL, Dixen K, Yadav R, Tygesen MP, Qvortrup K, Kristiansen K, Quistorff B, Gupta R, Wang
550 J, Hansen JB 2015 Global gene expression profiling of brown to white adipose tissue
551 transformation in sheep reveals novel transcriptional components linked to adipose remodeling.
552 BMC Genomics 16:215.
553 12. Mostyn A, Pearce S, Budge H, Elmes M, Forhead AJ, Fowden AL, Stephenson T, Symonds ME
554 2003 Influence of cortisol on adipose tissue development in the fetal sheep during late gestation. J
555 Endocrinol 176:23-30.
556 13. O' Connor DM, Blache D, Hoggard N, Brookes E, Wooding FBP, Fowden AL, Forhead AJ 2007
557 Developmental control of plasma leptin and adipose leptin messenger ribonucleic acid in the ovine
558 fetus during late gestation: role of glucocorticoids and thyroid hormones. Endocrinology 148:3750-
559 3757.
560 14. Schermer SJ, Bird JA, Lomax MA, Shepherd DA, Symonds ME 1996 Effect of fetal thyroidectomy
561 on brown adipose tissue and thermoregulation in newborn lambs. Reprod Fertil Dev 8:995-1002.
562 15. Gholami H, Jeddi S, Zadeh-Vakili A, Farrokhfall K, Rouhollah F, Zarkesh M, Ghanbari M,
563 Ghasemi A 2017 Transient congenital hypothyroidism alters gene expression of glucose
564 transporters and impairs glucose sensing apparatus in young and aged offspring rats. Cell Physiol
565 Biochem 43:2338-2352.
566 16. Tapia-Martínez J, Torres-Manzo AP, Franco-Colín M, Pineda-Reynoso M, Cano-Europa E 2019
567 Maternal thyroid hormone deficiency during gestation and lactation alters metabolic and thyroid
568 programming of the offspring in the adult stage. Horm Metab Res 51:381-388.
569 17. Obregón MJ 2014 Adipose tissues and thyroid hormones. Front Physiol 5:479.
570 18. Liu BX, Sun W, Kong XQ 2019 Perirenal fat: a unique fat pad and potential target for
571 cardiovascular disease. Angiology 70:584-593.
572 19. Hopkins PS, G.D. Thorburn 1972 The effects of foetal thyroidectomy on the development of
573 the ovine foetus. J Endocrinol 54:55-66.

574 20. Harris SE, De Blasio MJ, Davis MA, Kelly A, Davenport HM, Wooding FBP, Blache D, Meredith D,
575 Anderson M, Fowden AL, Limesand SW, Forhead AJ 2017 Hypothyroidism *in utero* stimulates
576 pancreatic beta cell proliferation and hyperinsulinaemia in the ovine fetus during late gestation. J
577 Physiol 595:3331-3343.
578 21. Blache D, Tellam RL, Chagas LM, Blackberry MA, Vercoe PE, Martin GB 2000 Level of nutrition
579 affects leptin concentrations in plasma and cerebrospinal fluid in sheep. J Endocrinol 165:625–637.
580 22. Forhead AJ, Jellyman JK, Gillham K, Ward JW, Blache D, Fowden AL 2011 Renal growth
581 retardation following angiotensin II type 1 (AT1) receptor antagonism is associated with increased
582 AT2 receptor protein in fetal sheep. J Endocrinol 208:137-145.
583 23. Karvonen MJ 1954 The diameter of foetal sheep erythrocytes. Acta Anat 20:53-61.
584 24. Ewels P, Krueger F, Käller M, Andrews S 2016 Cluster Flow: A user-friendly bioinformatics
585 workflow tool. Version 2. F1000Res 5:2824.
586 25. Andrews S, Krueger F, Degonds-Pichon A, Biggins L, Krueger C, Wingett S 2012 FastQC: a
587 quality control tool for high throughput sequence data. Available at:
588 http://www.bioinformatics.babraham.ac.uk/projects/fastqc.
589 26. Krueger F, Ewels P 2012 Trim Galore: A wrapper tool around Cutadapt and FastQC to
590 consistently apply quality and adapter trimming to FastQ files, with some extra functionality for
591 MspI-digested RRBS-type (Reduced Representation Bisufite-Seq) libraries. Available at:
592 https://www.bioinformatics.babraham.ac.uk/projects/trim_galore/.
593 27. Wingett SW, Andrews S 2018 FastQ Screen: A tool for multi-genome mapping and quality
594 control. F1000Res 7:1338.
595 28. Ewels P, Magnusson M, Lundin S, Käller M 2016 MultiQC: summarize analysis results for
596 multiple tools and samples in a single report. Bioinformatics 32:3047-3048.
597 29. Dobin A, Davis CA, Schlesinger F, Drenkow J, Zaleski C, Jha S, Batut P, Chaisson M, Gingeras TR
598 2013 STAR: ultrafast universal RNA-seq aligner. Bioinformatics 29:15-21.

599 30. Li H, Handsaker B, Wysoker A, Fennell T, Ruan J, Homer N, Marth G, Abecasis G, Durbin R 2009
600 1000 Genome Project Data Processing Subgroup, The Sequence Alignment/Map format and
601 SAMtools. Bioinformatics 25:2078-2079.
602 31. Liao Y, Smyth GK, Shi W 2013 The Subread aligner: fast, accurate and scalable read mapping by
603 seed-and-vote. Nucleic Acids Res 41:e108.
604 32. White P, Dauncey MJ 1999 Differential expression of thyroid hormone receptor isoforms is
605 strikingly related to cardiac and skeletal muscle phenotype during postnatal development. J Mol
606 Endocrinol 23:241-54.
607 33. The R Foundation 2018 The R Project for Statistical Computing. Available at: https://www.R-
608 project.org/.
609 34. Romero-Calvo I, Ocón B, Martínez-Moya P, Suárez MD, Zarzuelo A, Martínez-Augustin O, de
610 Medina FS 2010 Reversible Ponceau staining as a loading control alternative to actin in Western
611 blots. Anal Biochem 401:318-320.
612 35. Fowden AL, Silver M 1995 The effects of thyroid hormones on oxygen and glucose metabolism
613 in the sheep fetus during late gestation. J Physiol 482:203-13.36. Fowden AL, Hughes P, Comline
614 RS 1989 The effects of insulin on the growth rate of the sheep fetus during late gestation. Q J Exp
615 Physiol 74:703-714.
616 37. Mühlhäusler BS, Adam CL, Marrocco EM, Findlay PA, Roberts CT, McFarlane JR, Kauter KG,
617 McMillen IC 2005 Impact of glucose infusion on the structural and functional characteristics of
618 adipose tissue and on hypothalamic gene expression for appetite regulatory neuropeptides in the
619 sheep fetus during late gestation. J Physiol 565:185-195.
620 38. Carnevalli LS, Masuda K, Frigerio F, Le Bacquer O, Um SH, Gandin V, Topisirovic I, Sonenberg N,
621 Thomas G, Kozma SC 2010 S6K1 plays a critical role in early adipocyte differentiation. Dev Cell
622 18:763-774.
623 39. Lee MJ 2017 Hormonal regulation of adipogenesis. Compr Physiol 7:1151-1195.

624 40. Um SH, Sticker-Jantscheff M, Chau GC, Vintersten K, Mueller M, Gangloff YG, Adams RH, Spetz
625 JF, Elghazi L, Pfluger PT, Pende M, Bernal-Mizrachi E, Tauler A, Tschöp MH, Thomas G, Kozma SC
626 2015 S6K1 controls pancreatic β cell size independently of intrauterine growth restriction. J Clin
627 Invest 125:2736-2747.
628 41. Um SH, Frigerio F, Watanabe M, Picard F, Joaquin M, Sticker M, Fumagalli S, Allegrini PR,
629 Kozma SC, Auwerx J, Thomas G 2004 Absence of S6K1 protects against age- and diet-induced
630 obesity while enhancing insulin sensitivity. Nature 431:200-205.
631 2. Castelló A, Rodríguez-Manzaneque JC, Camps M, Pérez-Castillo A, Testar X, Palacín M, Santos A,
632 Zorzano A 1994 Perinatal hypothyroidism impairs the normal transition of GLUT4 and GLUT1
633 glucose transporters from fetal to neonatal levels in heart and brown adipose tissue. Evidence for
634 tissue-specific regulation of GLUT4 expression by thyroid hormone. J Biol Chem 269:5905-5912.
635 43. Forhead AJ, Li J, Saunders JC, Dauncey MJ, Gilmour RS, Fowden AL 2000 Control of ovine
636 hepatic growth hormone receptor and insulin-like growth factor I by thyroid hormones *in utero*.
637 Am J Physiol 278:E1166-1174.
638 44. Forhead AJ, Li J, Gilmour RS, Dauncey MJ, Fowden AL 2002 Thyroid hormones and the mRNA of
639 the GH receptor and IGFs in skeletal muscle of fetal sheep. Am J Physiol 282:E80-E86.
640 45. Devaskar SU, Anthony R, Hay W 2002 Ontogeny and insulin regulation of fetal ovine white
641 adipose tissue leptin expression. Am J Physiol 282:R431-R438.
642 46. Menendez C, Baldelli R, Camiña JP, Escudero B, Peino R, Dieguez C, Casanueva FF 2003 TSH
643 stimulates leptin secretion by a direct effect on adipocytes. J Endocrinol 176:7-12.
644 47. Obregón MJ, Calvo R, Hernández A, Escobar del Rey F, Morreale de Escobar G 1996 Regulation
645 of uncoupling protein messenger ribonucleic acid and 5'-deiodinase activity by thyroid hormones
646 in fetal brown adipose tissue. Endocrinology 137:4721-4729.

647 48. Guerra C, Roncero C, Porras A, Fernández M, Benito M 1996 Triiodothyronine induces the
648 transcription of the uncoupling protein gene and stabilizes its mRNA in fetal rat brown adipocyte
649 primary cultures. J Biol Chem 271:2076-2081.
650 49. Villarroya F, Peyrou M, Giralt M 2017 Transcriptional regulation of the uncoupling protein-1
651 gene. Biochimie 134:86-92.
652 50. Walker DW, Schuijers JA 1989 Effect of thyroidectomy on cardiovascular responses to hypoxia
653 and tyramine infusion in fetal sheep. J Dev Physiol 12:337-345.
654 51. Klein AH, Reviczky A, Padbury JF 1984 Thyroid hormones augment catecholamine-stimulated
655 brown adipose tissue thermogenesis in the ovine fetus. Endocrinology 114:1065-1069.
656 52. Moog NK, Entringer S, Heim C, Wadhwa PD, Kathmann N, Buss C 2017 Influence of maternal
657 thyroid hormones during gestation on fetal brain development. Neuroscience 342:68-100.
658 53. Wu SY, Merryfield ML, Polk DH, Fisher DA 1990 Two pathways for thyroxine 5'-
659 monodeiodination in brown adipose tissue in fetal sheep: ontogenesis and divergent responses to
660 hypothyroidism and 3,5,3'-triiodothyronine replacement. Endocrinology 126:1950-1958.
661 54. Forhead AJ, Curtis K, Kaptein E, Visser TJ, Fowden AL 2006 Developmental control of
662 iodothyronine deiodinases by cortisol in the ovine fetus and placenta near term. Endocrinology
663 147:5988-5994.
664 55. Polk DH, Wu SY, Wright C, Reviczky AL, Fisher DA 1988 Ontogeny of thyroid hormone effect on
665 tissue 5'-monodeiodinase activity in fetal sheep. Am J Physiol 254:E337-E341.
666 56. Toyoda N, Zavacki AM, Maia AL, Harney JW, Larsen PR 1995 A novel retinoid X receptor-
667 independent thyroid hormone response element is present in the human type 1 deiodinase gene.
668 Mol Cell Biol 15:5100-5112.
669 57. Catalano PM, Presley L, Minium J, Hauguel-de Mouzon S 2009 Fetuses of obese mothers
670 develop insulin resistance *in utero*. Diabetes Care 32:1076-1080.

671 58. Catalano PM, Farrell K, Thomas A, Huston-Presley L, Mencin P, de Mouzon SH, Amini SB 2009
672 Perinatal risk factors for childhood obesity and metabolic dysregulation. Am J Clin Nutr 90:1303-
673 1313.
674 59. Aiceles V, Gombar FM, Cavalcante FDS, Ramos CDF 2019 Congenital hypothyroidism is
675 associated with impairment of the leptin signaling pathway in the hypothalamus in male Wistar
676 animals in adult life. Horm Metab Res 51:330-335.
677

678 **Figure Legends**

679 1. Mean (± SEM) measurements of (A) perirenal adipose tissue (PAT) composition, (B) relative PAT
680 mass and (C) unilocular (UL) adipocyte perimeter in sham and thyroidectomised (TX) fetuses at
681 129 and 143 days of gestation (dGA). * Significantly different from sham fetuses at same
682 gestational age; + significantly different from fetuses at 129 dGA in the same treatment group,
683 $P<0.05$. Representative histological images of perirenal adipose tissue taken from (D) sham and
684 (E) TX sheep fetuses at 143 dGA. Haematoxylin and eosin stain.

685

686 2. KEGG pathway and biological process (BP) bar plots using RNA-sequencing data from perirenal
687 adipose tissue taken from sham and thyroidectomised (TX) fetuses at 129 and 143 days of
688 gestation (dGA). Selected relevant KEGG (A) and BP ontology (B) pathway bar plots indicating the
689 number of up and down-regulated genes when the data were compared by treatment (TX and
690 sham); the red and blue bars represent up and down-regulated genes, respectively.

691

692 3. Mean (± SEM) abundance of (A) uncoupling protein-1 (UCP1) mRNA, (B) UCP1 mRNA relative to
693 the percentage volume of multilocular (ML) adipose tissue, and (C) UCP1 protein relative to the
694 percentage volume of ML adipose tissue and (D) citrate synthase (CS) activity, in perirenal adipose
695 tissue taken from sham and thyroidectomised (TX) fetuses at 129 and 143 days of gestation (dGA).
696 * Significantly different from sham fetuses at same gestational age; + significantly different from
697 fetuses at 129 dGA in the same treatment group, $P<0.05$. AU, arbitrary units.

698

699 4. Mean (± SEM) mRNA abundance of (A) iodothyronine deiodinase-1 (DIO1), (B) DIO2, (C) thyroid
700 hormone receptor α1 (TRα1), (D) TRα2 and (E) TRβ in perirenal adipose tissue taken from sham
701 and thyroidectomised (TX) fetuses at 129 and 143 days of gestation (dGA). * Significantly different

from sham fetuses at same gestational age; + significantly different from fetuses at 129 dGA in the same treatment group, P<0.05. AU, arbitrary units.

Supplementary Figure Legends

S1. Principal component analysis (PCA)-based clustering, PC1 and PC2, and heatmap plots using RNA-sequencing data from perirenal adipose tissue taken from sham and thyroidectomised (TX) fetuses at 129 and 143 days of gestation (dGA). (A) Unbiased PCA-based clustering of treatment (TX and sham) with gestational age (129 and 143 dGA). The 500 most variable genes and the two principal components were used for clustering and to describe the variance between the subsets. (B) Top 25 genes that explained the variance by treatment (TX and sham) within PC1. (C) Top 25 genes that explained the variance by gestational age (129 and 143 dGA) within PC2. (D) Clustering heatmap analysis for the top 272 genes under the DESeq2 comparison by treatment (TX and sham) with Padj < 0.05 and absolute log2 fold change ≥ 2.

S2. Volcano plots using RNA-sequencing data from perirenal adipose tissue taken from sham and thyroidectomised (TX) fetuses at 129 and 143 days of gestation (dGA). Volcano plots comparing data by treatment (A: TX and sham) and gestational age (B: 129 and 143 dGA), and between and within treatment and gestational age groups (C-F). Red and blue dots represent up and down-regulated differentially expressed genes, respectively (absolute log2 fold change ≥ 1, Padj < 0.05).

S3. Differentially expressed gene (DEG) intersection plot using RNA-sequencing data from perirenal adipose tissue taken from sham and thyroidectomised (TX) fetuses at 129 and 143 days of gestation (dGA). (A) Number of significant DEGs, with an absolute log2 fold change ≥ 1, Padj < 0.05, identified from comparisons between and within treatment and gestational age groups. (B) Number of unique significant DEGs for each comparison.

S4. KEGG pathway heatmap and bar plot using RNA-sequencing data from perirenal adipose tissue taken from sham and thyroidectomised (TX) fetuses at 129 and 143 days of gestation (dGA). (A) KEGG pathway heatmap for data stratified by treatment and gestational age, and between and within treatment and gestational age groups. (B) KEGG pathway bar plot indicating the number of up and down-regulated genes when the data were compared by treatment (TX and sham); the red and blue bars represent up and down-regulated genes, respectively.

S5. Biological process (BP) ontology pathway bar plot using RNA-sequencing data from perirenal adipose tissue taken from sham and thyroidectomised (TX) fetuses at 129 and 143 days of gestation (dGA). (A) BP ontology pathway heatmap for data stratified by treatment and gestational age, and between and within treatment and gestational age groups. (B) BP ontology pathway bar plot indicating the number of up and down-regulated genes when the data were compared by treatment (TX and sham); the red and blue bars represent up and down-regulated genes, respectively.

S6. Mean (± SEM) mRNA and protein abundance of (Ai, ii) proliferating cell nuclear antigen (PCNA), (Bi, ii) peroxisome proliferator-activated receptor γ (PPARγ), (Ci, ii) insulin receptor (InsR), (Di, ii) protein kinase β 1 (Akt1), (Ei, ii) Akt2, (Fi, ii) mammalian target of rapamycin (mTOR, phosphorylated protein), (Gi, ii) S6 kinase (S6K, phosphorylated protein) and (Hi, ii) glucose transporter-4 (GLUT4), in perirenal adipose tissue taken from sham and thyroidectomised (TX) fetuses at 129 and 143 days of gestation (dGA). * Significantly different from sham fetuses at same gestational age; + significantly different from fetuses at 129 dGA in the same treatment group, $P<0.05$. AU, arbitrary units.

S7. Mean (± SEM) mRNA abundance of (A) insulin-like growth factor-I (IGFI), (B) IGFII, (C) leptin and the adrenergic receptors (D) α1A, (E) α1D, (F) α2A, (G) β1, (H) β2 and (I) β3 in perirenal adipose tissue taken from sham and thyroidectomised (TX) fetuses at 129 and 143 days of gestation (dGA). * Significantly different from sham fetuses at same gestational age; + significantly different from fetuses at 129 dGA in the same treatment group, $P<0.05$. AU, arbitrary units.

S8. A Sashimi plot to show the expression of differentially spliced transcripts of the thyroid hormone receptor (TR), TRα1 and TRα2, in perirenal adipose tissue taken from sham and thyroidectomised (TX) fetuses at 129 and 143 days of gestation (dGA). The annotation bars represent TRα1 in red and TRα2 in green.

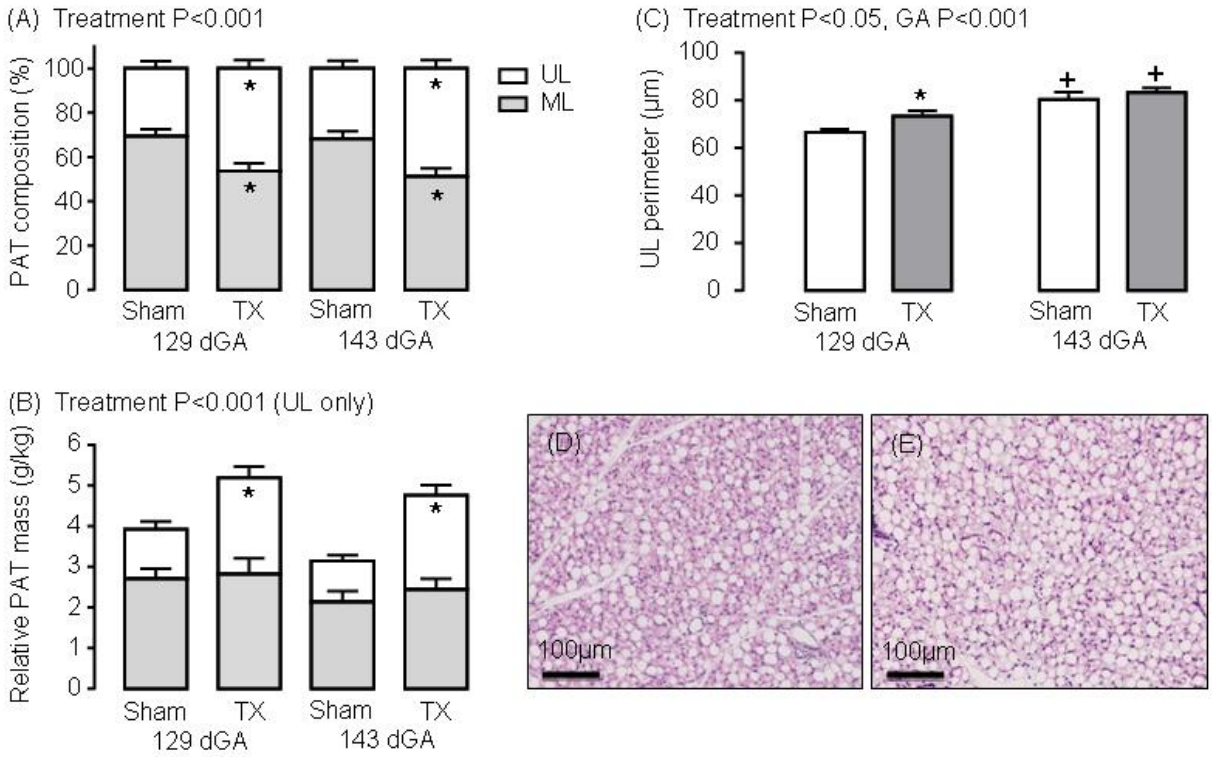

764

765 **Figure 1**
766

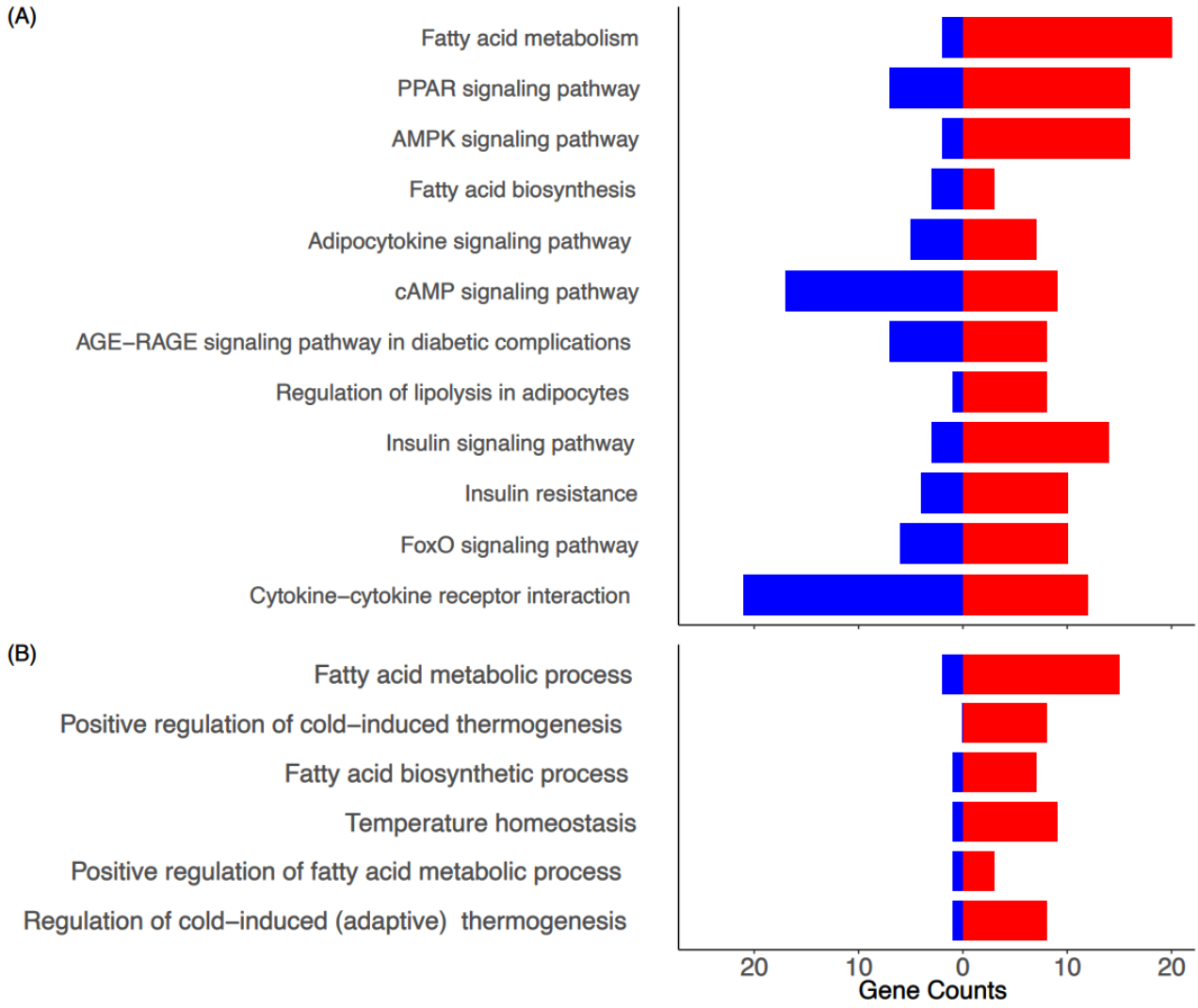
(A)
Fatty acid metabolism
PPAR signaling pathway
AMPK signaling pathway
Fatty acid biosynthesis
Adipocytokine signaling pathway
cAMP signaling pathway
AGE−RAGE signaling pathway in diabetic complications
Regulation of lipolysis in adipocytes
Insulin signaling pathway
Insulin resistance
FoxO signaling pathway
Cytokine−cytokine receptor interaction
(B)
Fatty acid metabolic process
Positive regulation of cold−induced thermogenesis
Fatty acid biosynthetic process
Temperature homeostasis
Positive regulation of fatty acid metabolic process
Regulation of cold−induced (adaptive) thermogenesis
20
10
0
10
20
Gene Counts

Figure 2

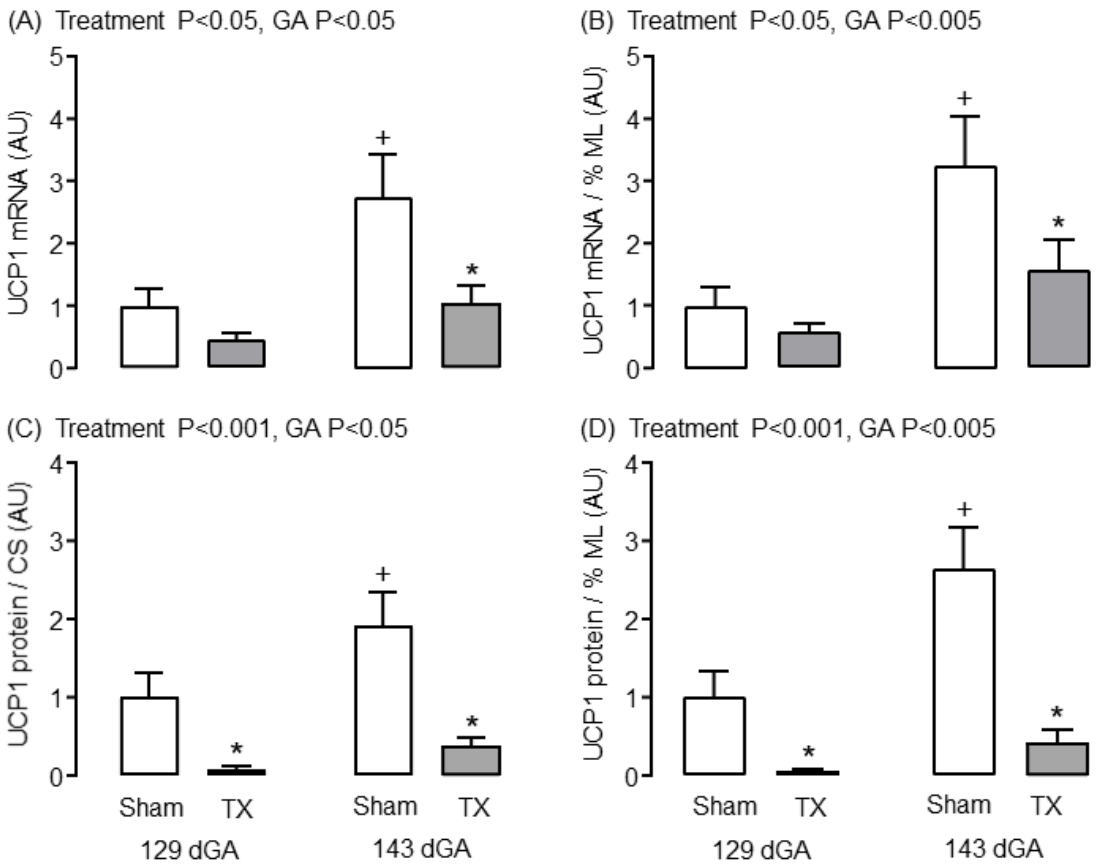
(A) Treatment P<0.05, GA P<0.05
UCP1 mRNA (AU)
(B) Treatment P<0.05, GA P<0.005
UCP1 mRNA / % ML (AU)
(C) Treatment P<0.001, GA P<0.05
UCP1 protein / CS (AU)
(D) Treatment P<0.001, GA P<0.005
UCP1 protein / % ML (AU)
Sham
TX
129 dGA
143 dGA

Figure 3

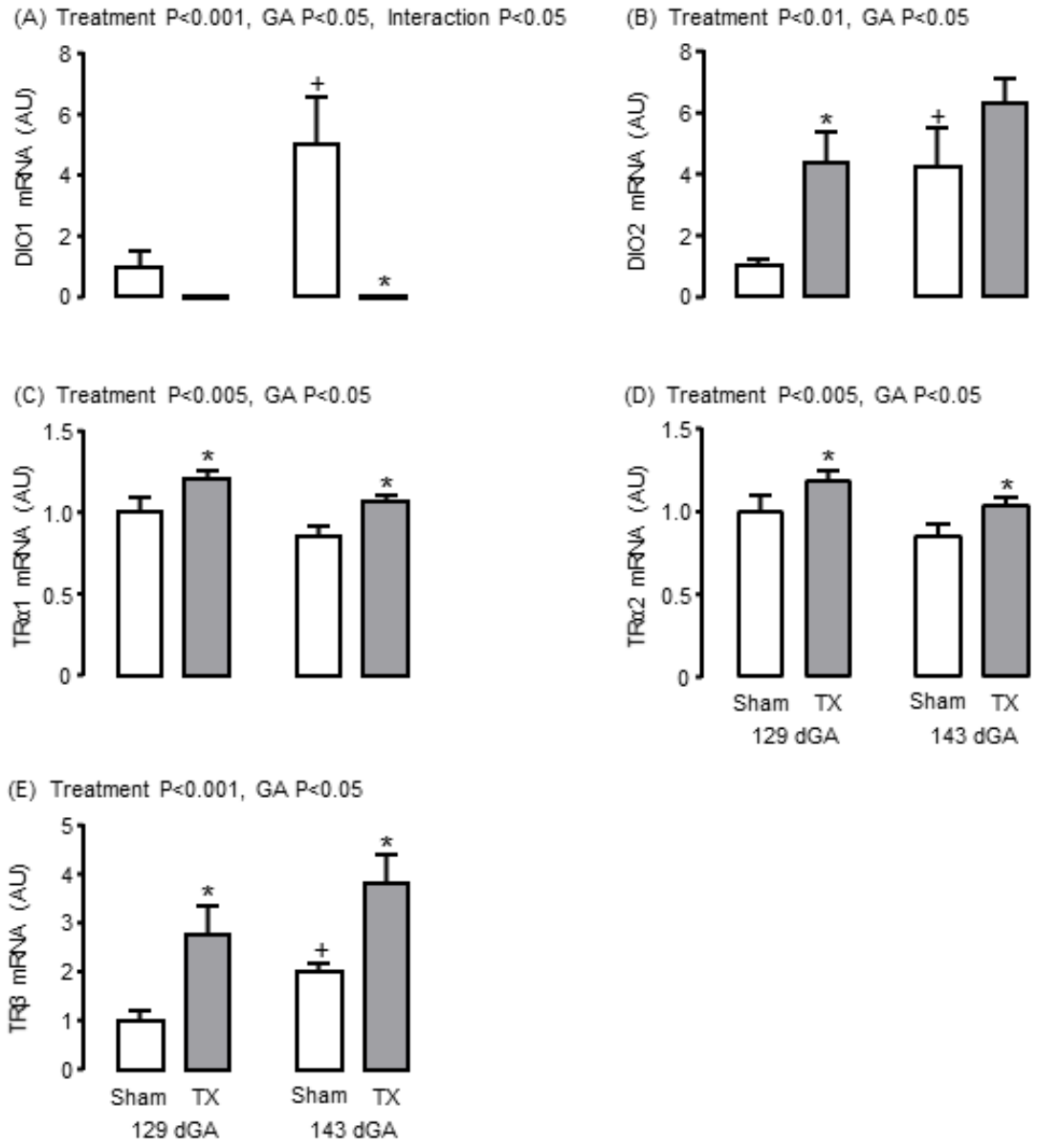

773
774 **Figure 4**
775

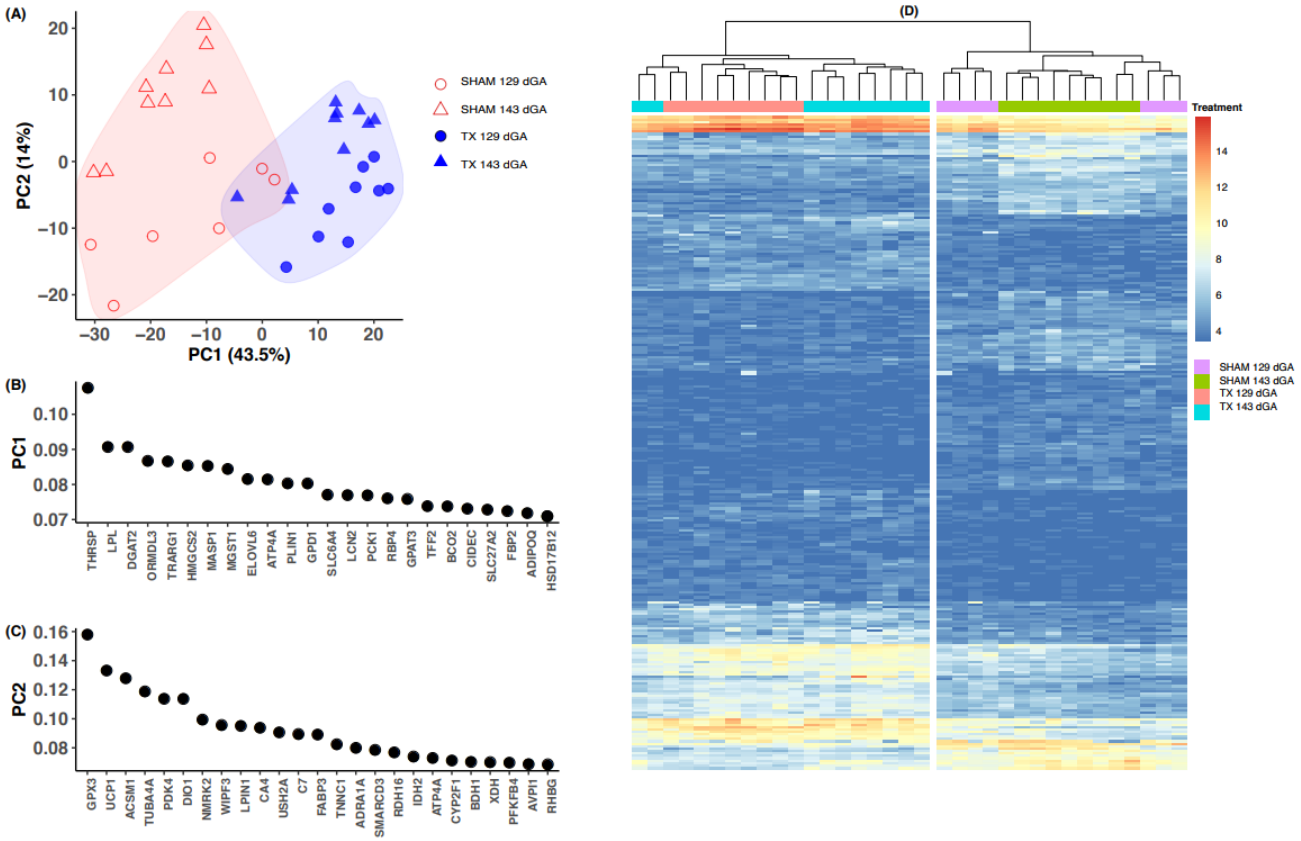

Supplementary Figure S 1

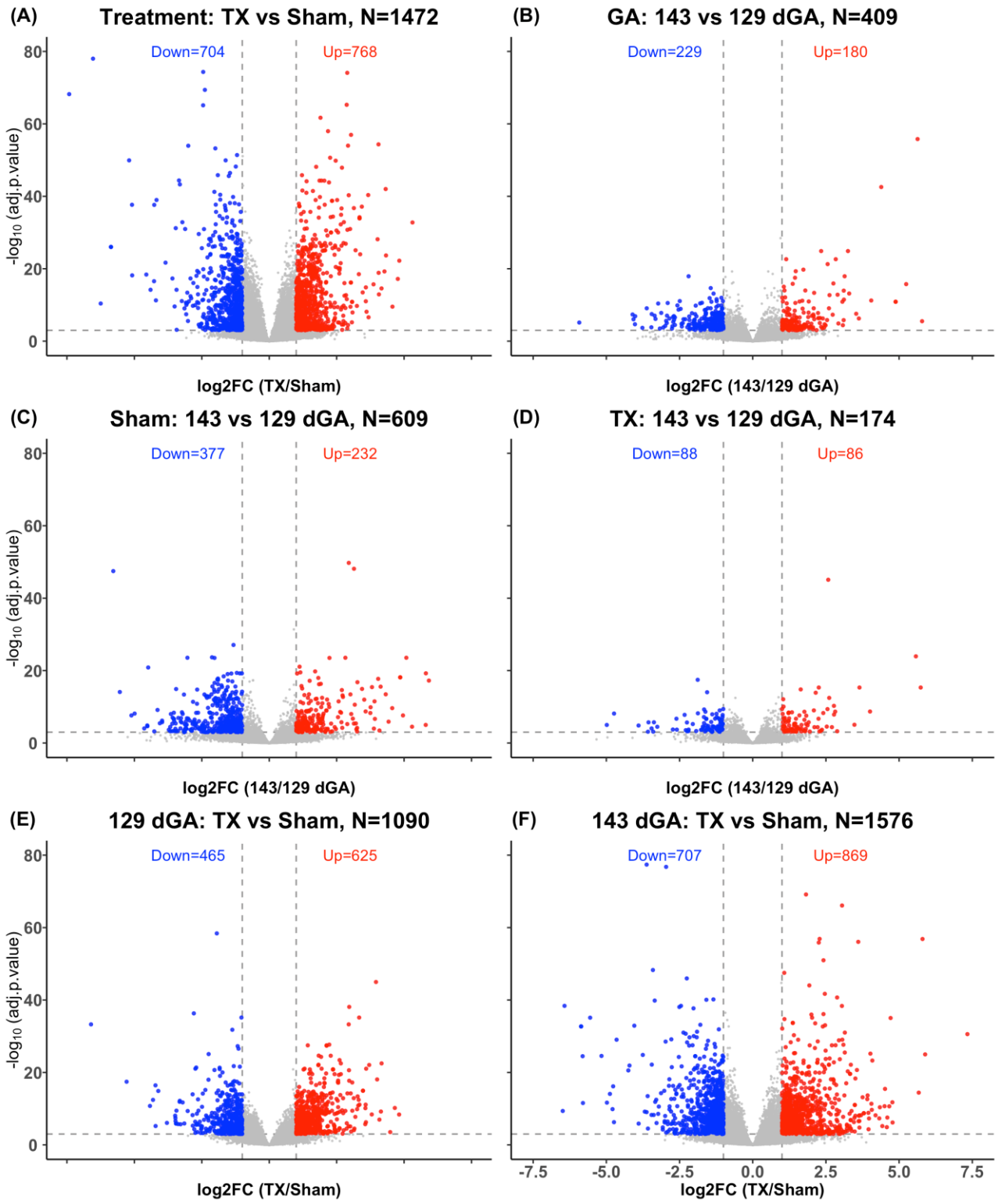

Supplementary Figure S 2

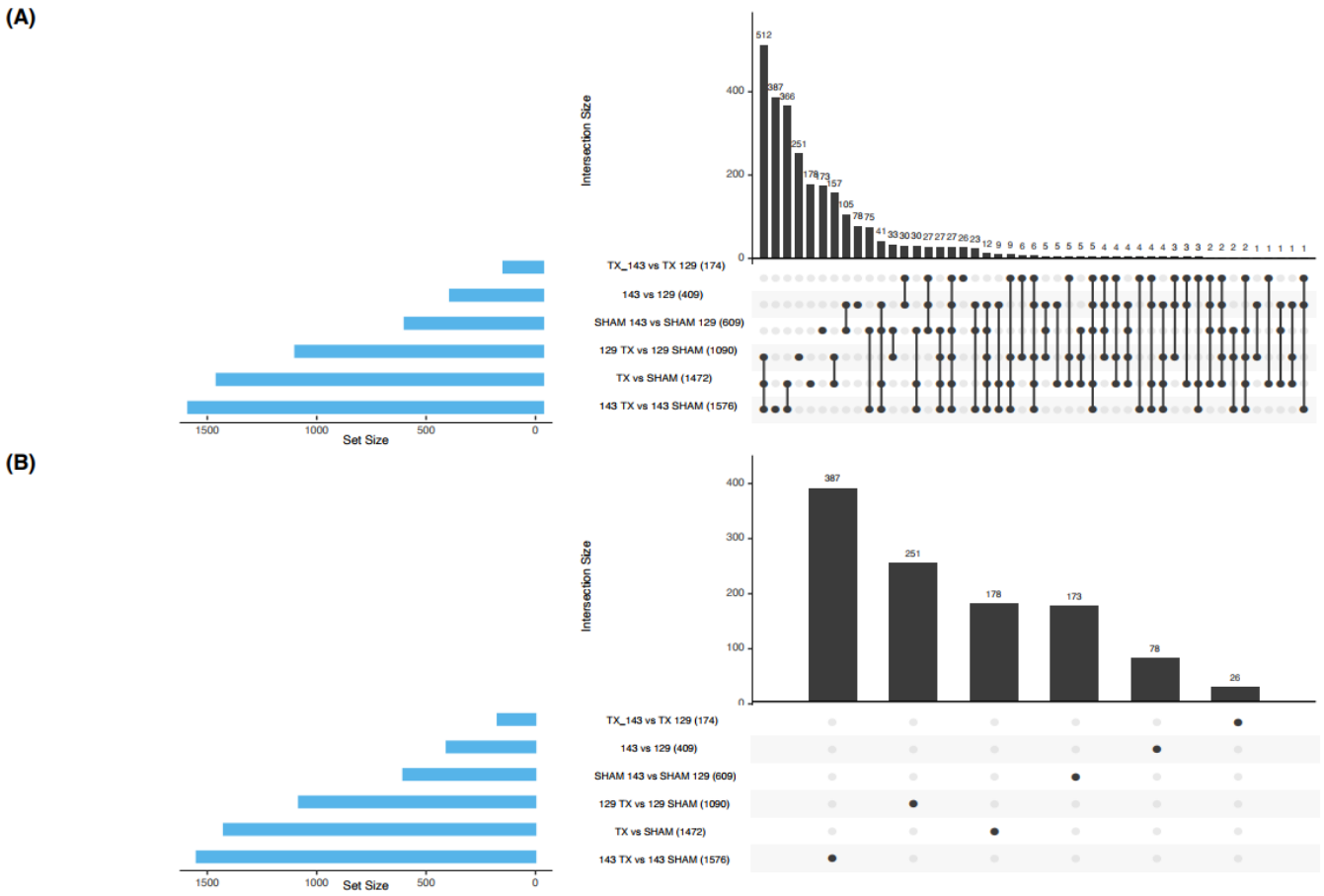

Supplementary Figure S 3

Supplementary Figure S 4A

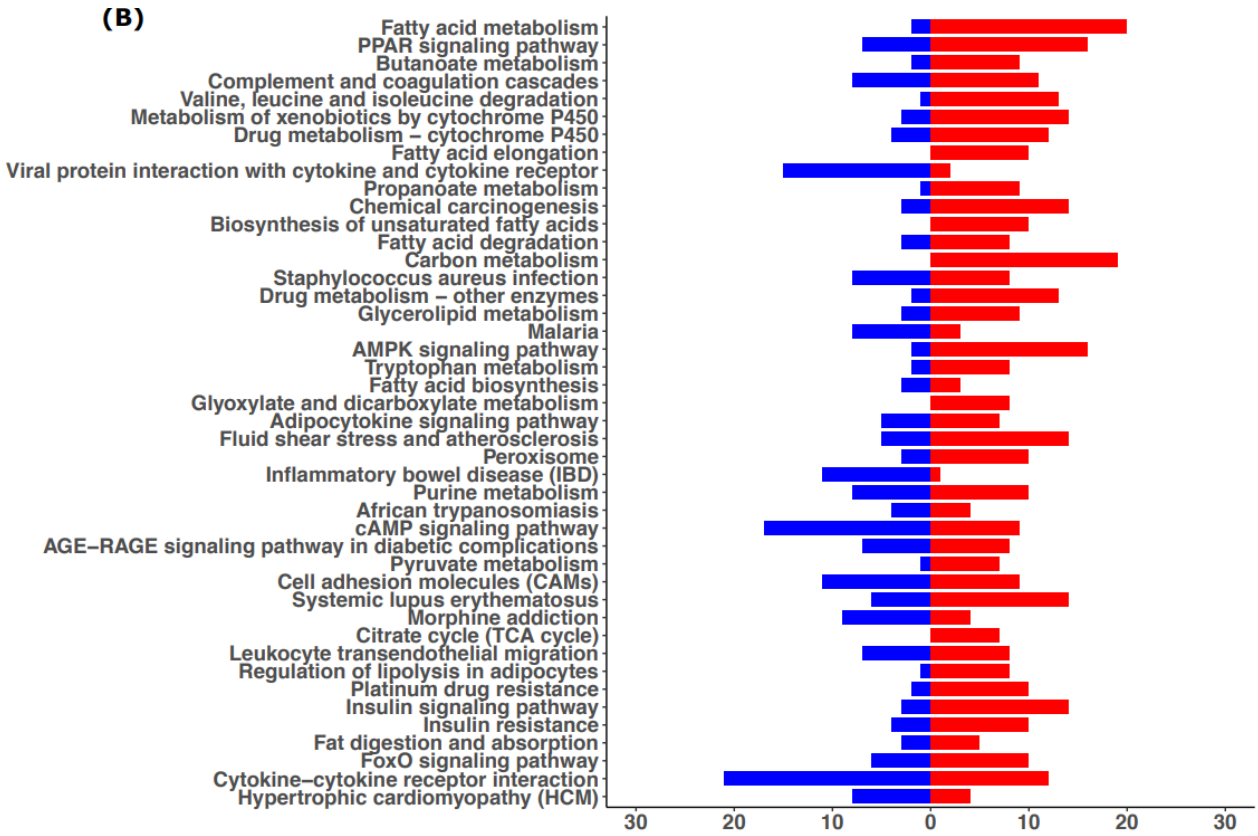

Supplementary Figure S4B

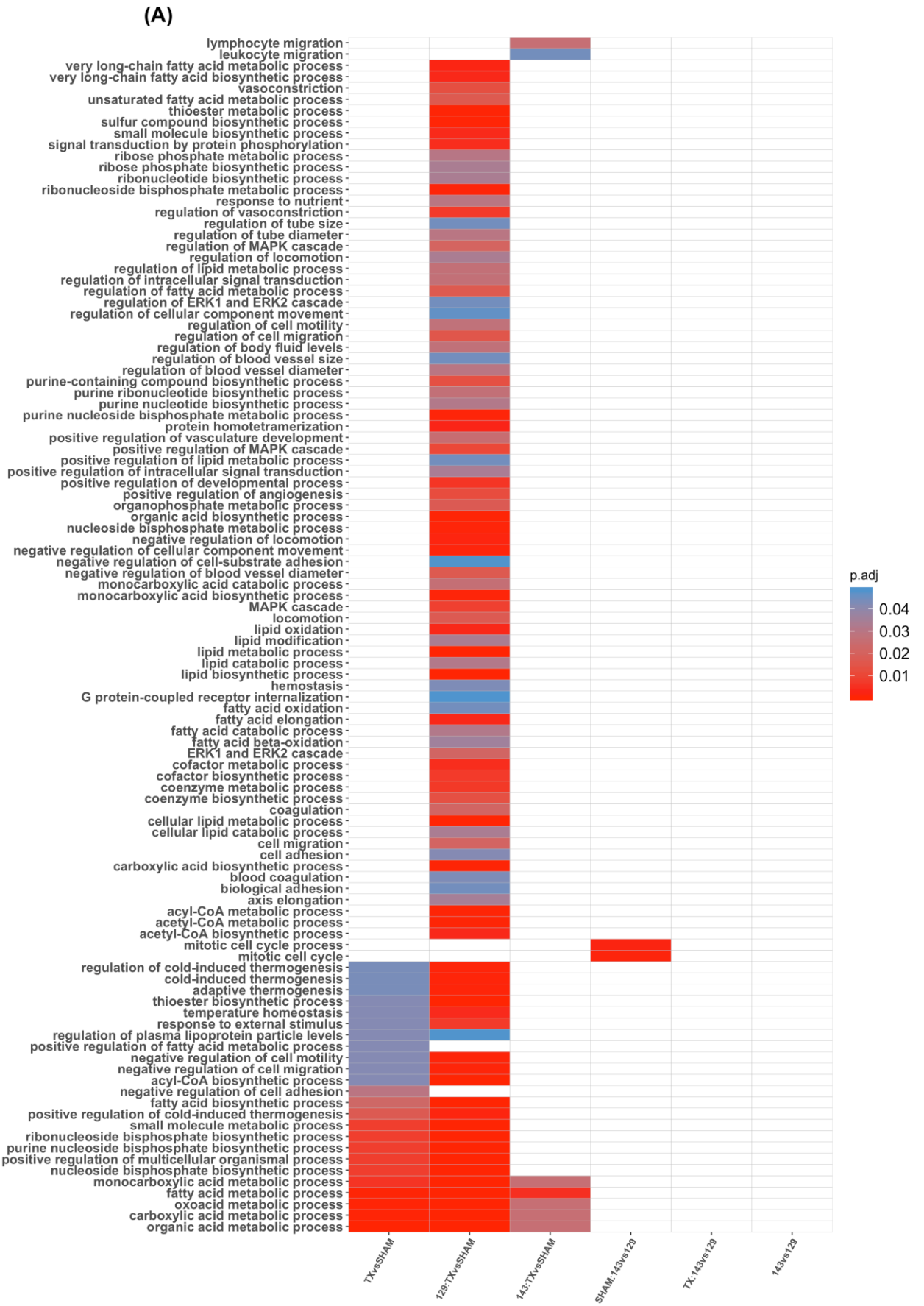

Supplementary Figure S5A

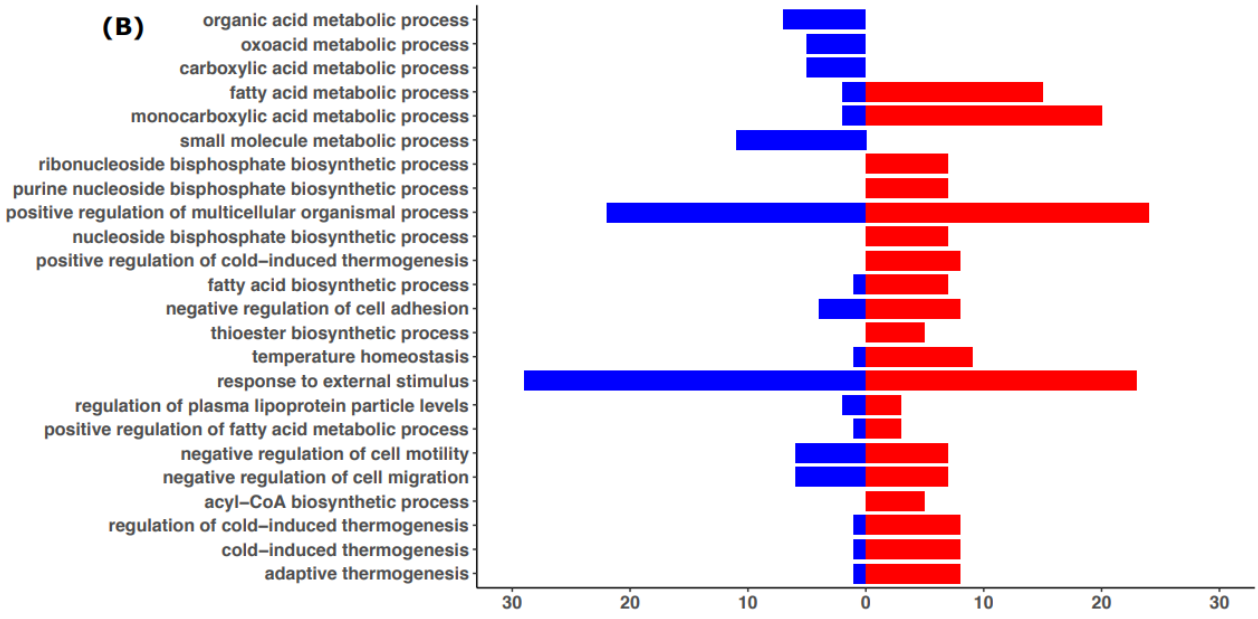

Supplementary Figure S5B

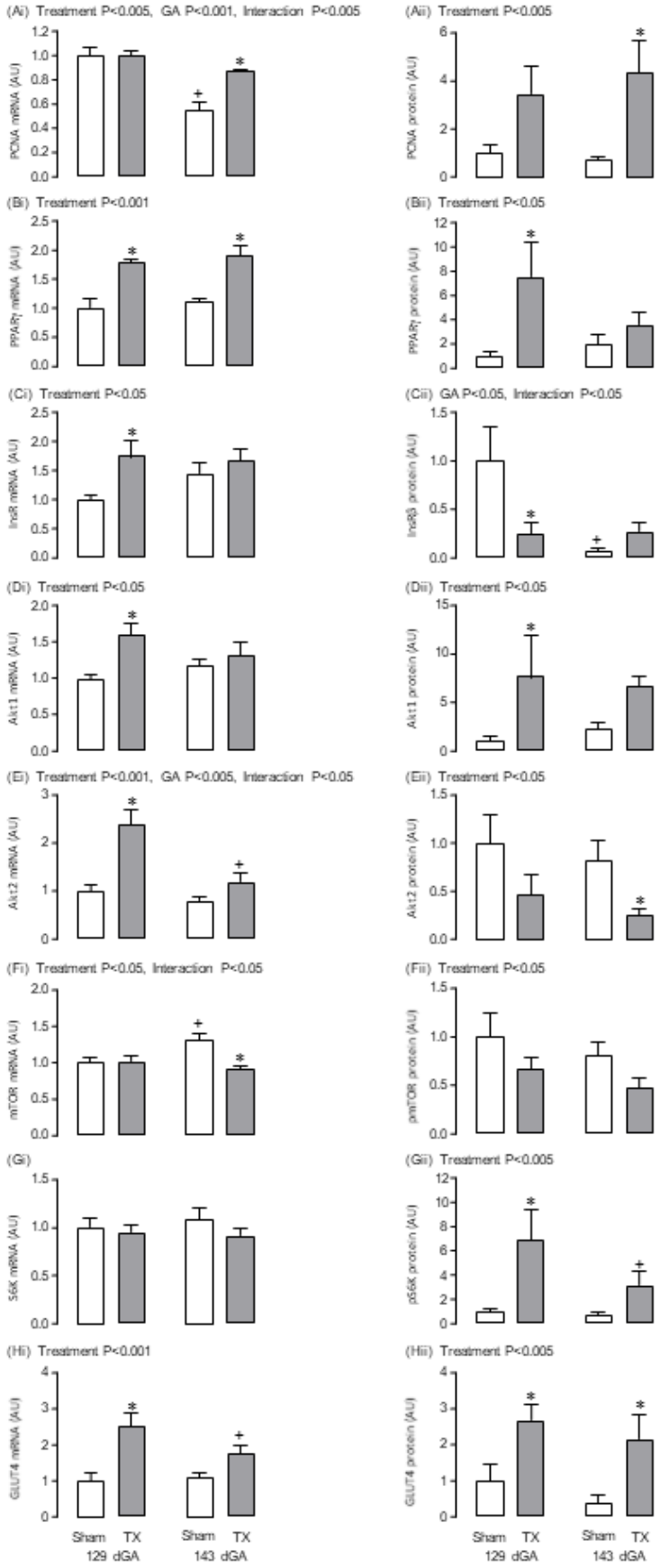

Supplementary Figure S6

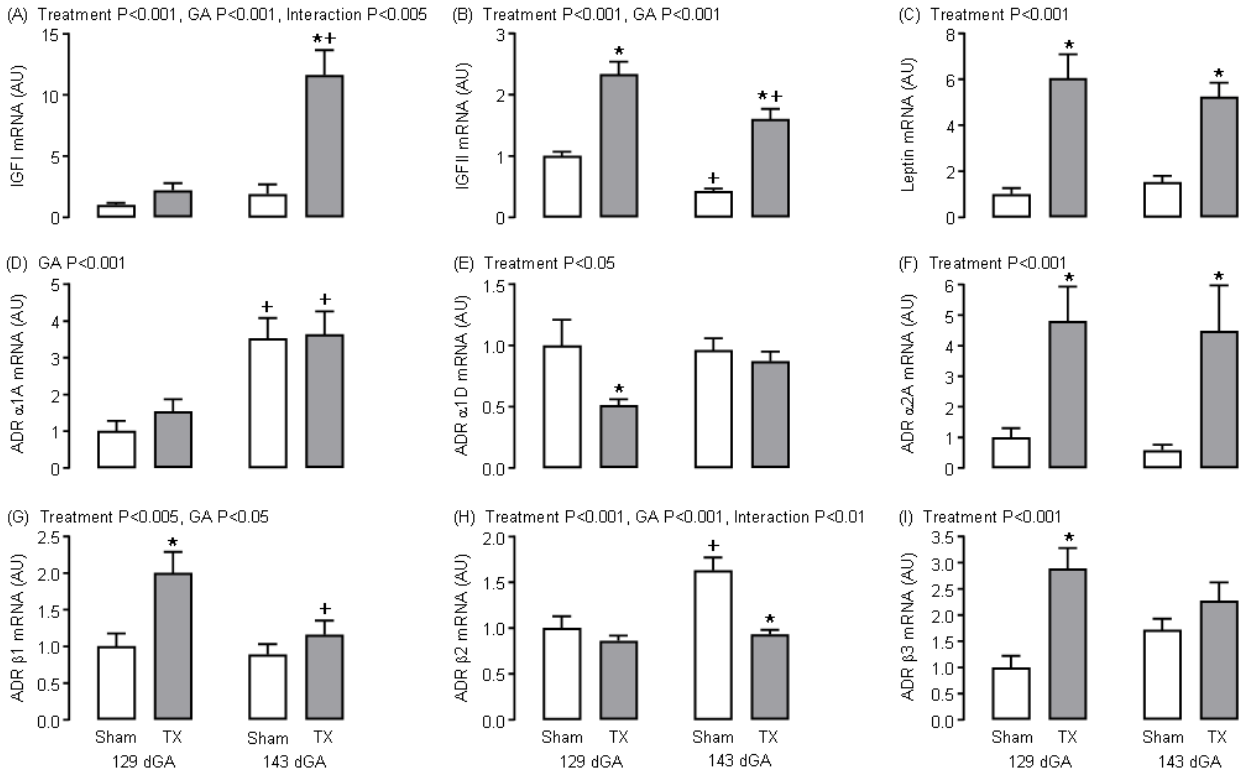

Supplementary Figure S7

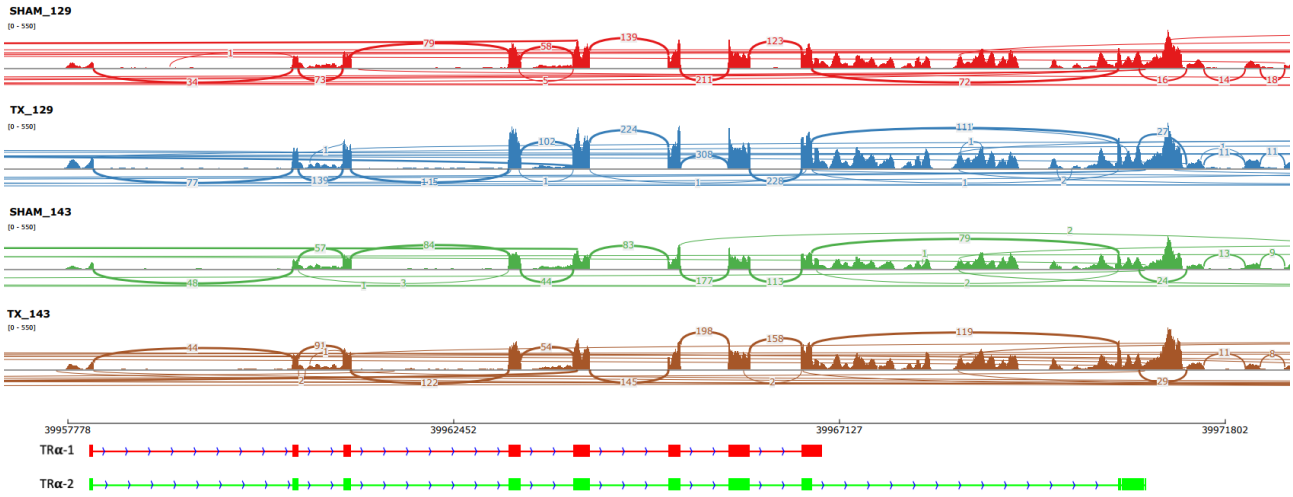

Supplementary Figure S8